Specific immune modulation of experimental colitis drives enteric alpha-synuclein accumulation and triggers age-related Parkinson-like brain pathology

Stefan Grathwohl
Roche Pharma Schweiz AG
Emmanuel Quansah
VARI: Van Andel Research Institute
Nazia Maroof
Roche Pharma AG
Jennifer A Steiner
VARI: Van Andel Research Institute
Liz Spycher
Roche Pharma AG
Fethallah Benmansour
Roche Pharma AG
Gonzalo Duran-Pacheco
Roche Pharma AG
Juliane Siebourg-Polster
Roche Pharma AG
Krisztina Oroszlan-Szovik
Roche Pharma AG
Helga Remy
Roche Pharma AG
Markus Haenggi
Roche Pharma AG
Marc Stawiski
Roche Pharma AG
Matthias Selhausen
Roche Pharma AG
Pierre Maliver
Roche Pharma AG
Andreas Wolfert
Roche Diagnostics GmbH
Thomas Emrich

Roche Diagnostics GmbH
Zachary Madaj
VARI: Van Andel Research Institute
Arel Su
Roche Pharma AG
Martha L Escobar Galvis
VARI: Van Andel Research Institute
Christoph Mueller
University of Berne Institute of Pathology: Universitat Bern Institut fur Pathologie
Annika Herrmann
Roche Pharma AG
Patrik Brundin
VARI: Van Andel Research Institute
Markus Britschgi (markus.britschgi@roche.com)
Hoffmann-La Roche https://orcid.org/0000-0001-6151-4257

Research article

Keywords: Parkinson's disease, colitis, enteric nervous system, peripheral inflammation, α-synuclein 92 pathology, neurodegeneration, translational mouse model

Posted Date: November 3rd, 2020

DOI: https://doi.org/10.21203/rs.3.rs-100199/v1

Specific immune modulation of experimental colitis drives enteric alpha-synuclein accumulation and triggers age-related Parkinson-like brain pathology

Stefan Grathwohl[1], Emmanuel Quansah[2], Nazia Maroof[1], Jennifer A. Steiner[2], Liz Spycher[1], Fethallah Benmansour[3], Gonzalo Duran-Pacheco[4], Juliane Siebourg-Polster[4], Krisztina Oroszlan-Szovik[1], Helga Remy[1], Markus Haenggi[1], Marc Stawiski[1], Matthias Sehlhausen[4], Pierre Maliver[4], Andreas Wolfert[5], Thomas Emrich[5], Zachary Madaj[2], Arel Su[4], Martha L. Escobar Galvis[2], Christoph Mueller[6], Annika Herrmann[4], Patrik Brundin[2]*, and Markus Britschgi[1]*

[1] Roche Pharma Research and Early Development, Neuroscience and Rare Diseases Research, Roche Innovation Center Basel, F. Hoffmann-La Roche Ltd, Grenzacherstrasse 124, Basel, Switzerland

[2] Center for Neurodegenerative Science, Van Andel Research Institute, 333 Bostwick Ave. NE, Grand Rapids, MI, USA

[3] Roche Pharma Research and Early Development, pREDi, Roche Innovation Center Basel, F. Hoffmann-La Roche Ltd, Grenzacherstrasse 124, Basel, Switzerland

[4] Roche Pharma Research and Early Development, Pharmaceutical Sciences, Roche Innovation Center Basel, F. Hoffmann-La Roche Ltd, Grenzacherstrasse 124, Basel, Switzerland

[5] Roche Pharma Research and Early Development, Pharmaceutical Sciences, Roche Innovation Center Munich, Roche Diagnostics GmbH, Nonnenwald 2, Penzberg, Germany

[6] Institute of Pathology, University of Bern, Murtenstrasse 31, Bern, Switzerland

Corresponding authors:

* Markus Britschgi, Roche Pharma Research and Early Development, Neuroscience and Rare Diseases Research, Roche Innovation Center Basel, F. Hoffmann-La Roche Ltd, Grenzacherstrasse 124, 4070 Basel, Switzerland

Tel: +41 61 6879116

Email: markus.britschgi@roche.com

* Patrik Brundin, Van Andel Institute, 333 Bostwick Ave. NE, Grand Rapids, MI 49503, USA.

Tel: +1 616.234.5312

Email: patrik.brundin@vai.org

Current email addresses of all co-authors:

Stefan Grathwohl, S.Grathwohl@gmx.de
Emmanuel Quansah, Emmanuel.Quansah@vai.org
Nazia Maroof, naziamaroof@yahoo.co.uk
Jennifer Steiner, Jennifer.Steiner@vai.org
Liz Spycher, liz.spycher@gmail.com
Fethallah Benmansour, fethallah.benmansour@roche.com
Gonzalo Duran-Pacheco, gonzalo_christian.duran_pacheco@roche.com
Juliane Siebourg-Polster, juliane.siebourg-polster@roche.com
Krisztina Oroszlan-Szovik, krisztina.oroszlan@bluewin.ch
Helga Remy, helga.remy@roche.com
Markus Haenggi, markus.haenggi@sunrise.ch
Marc Stawiski, marc.stawiski@gmail.com
Matthias Selhausen, matthias.selhausen@roche.com
Pierre Maliver, pierre.maliver@roche.com
Andreas Wolfert, andreas.wolfert@roche.com
Thomas Emrich, thomas.emrich@roche.com
Zachary Madaj, Zachary.Madaj@vai.org
Arel Su, arel.su@roche.com
Martha Escobar, Martha.Escobar@vai.org
Christoph Mueller, christoph.mueller@pathology.unibe.ch
Annika Herrmann, annika@bridgepathology.com
Patrik Brundin, Patrik.Brundin@vai.org
Markus Britschgi, markus.britschgi@roche.com

Abstract

Background: Intraneuronal accumulation of α-synuclein (αSyn) is key in Parkinson's disease (PD) pathogenesis. The pathogenic process is suggested to begin in the enteric nervous system decades before diagnosis of PD and then propagate into the brain. The triggers for these events are unclear but, in some patients, colitis might play a critical role.

Methods: We administered lipopolysaccharide (LPS) or dextran sulfate sodium (DSS) to assess the effect of different types of experimental colitis on αSyn accumulation in the gut of αSyn transgenic and wild type mice and quantified local gene expression by RT-PCR and level of αSyn accumulation by immunofluorescence imaging. Immune modulation during the DSS colitis paradigm in the αSyn transgenic mice included genetic ablation of Cx3cr1 or treatment with recombinant IL-10. To determine long-term effects of experimental colitis, we induced DSS colitis in young αSyn transgenic mice and aged them under normal conditions up to nine or 21 months before analyzing their brains by immunohistochemistry. In vivo experiments were performed in randomized cohorts. Blinded experimenters performed image analysis and statistical analysis depended on data type (i.e., Student's t-test, ANOVA, mixed-effects model).

Results: We demonstrate that mild sustained or one strong insult of experimental DSS colitis triggers αSyn accumulation in the submucosal plexus of wild type and αSyn transgenic mice, while short-term mild DSS experimental colitis or inflammation induced by LPS does not have such an effect. Lack of macrophage-related Cx3cr1-signalling during DSS colitis increases accumulation of αSyn in the colonic submucosal plexus of αSyn transgenic mice while systemic treatment with immune-dampening IL-10 ameliorates this phenomenon. Additionally, DSS colitis-induced αSyn accumulation in young αSyn transgenic mice persists for months and is exacerbated by lack of Cx3cr1-signaling. Remarkably, experimental colitis at three months of age exacerbates the accumulation of aggregated phospho-Serine 129 αSyn in the midbrain (including the substantia nigra), in 21- but not 9-month-old αSyn transgenic mice. This increase in midbrain αSyn accumulation is accompanied by the loss of tyrosine hydroxylase-immunoreactive nigral neurons.

Conclusions: Our data suggest that specific types of intestinal inflammation, mediated by monocyte/macrophage signaling, could play a critical role in the initiation and progression of PD.

Keywords: Parkinson's disease; colitis; enteric nervous system; peripheral inflammation; α-synuclein pathology; neurodegeneration; translational mouse model

Background

Parkinson's disease (PD) is a progressively debilitating neurodegenerative disease affecting 1% of the population above 60 years [1]. Typical symptoms are motor impairments including muscle rigidity, tremor, and bradykinesia. Neuropathologically, PD is hallmarked by loss of dopaminergic neurons in the substantia nigra (SN), a concomitant reduction of striatal dopaminergic signaling [2], and the presence of intraneuronal inclusions called Lewy bodies and neurites [3]. Lewy pathology is enriched in α-synuclein (αSyn), a presynaptic protein that tends to aggregate and become phosphorylated under pathological conditions [2]. Rare point mutations in αSyn and gene multiplications also cause familial forms of PD and related neurological conditions, and certain single nucleotide polymorphisms close to the αSyn gene (*SNCA*) locus are associated with increased risk for sporadic PD [4]. These findings make αSyn a focal point of biomarker and drug development programs for PD.

Several years before the first appearance of motor symptoms, many patients exhibit a variety of non-motor symptoms including constipation, sleep disorder, depression, and hyposmia [5–7]. Indeed, co-occurrence of some of these non-motor symptoms is coupled to elevated PD risk [8–11]. Constipation is an important non-motor feature of prodromal PD, with 28-61% of patients having exhibited gastrointestinal dysfunction for several years during the prodrome [7,10,12]. Notably, αSyn-immunoreactive inclusions have been found in neurons of the submucosal plexus in people with PD [3,13]. Taken together, this converging evidence suggests an early involvement of the enteric nervous system (ENS) in the pathogenesis of PD. Already over a decade ago, Braak and colleagues hypothesized that αSyn-immunoreactive inclusions first appear in the ENS and then occur in the parasympathetic (e.g., vagal output neurons in the intestines) and sympathetic (e.g., in the celiac ganglion in the upper abdomen) nervous system and gradually engage the brainstem, including the vagal dorsal motor nucleus and midbrain areas [3,13]. Several studies in preclinical models have demonstrated that αSyn pathology in the gut is associated with the development of αSyn pathology in the brain [14–20]. For a better understanding of PD pathogenesis and particularly events happening at preclinical stages of PD, it is critical to determine factors that regulate αSyn accumulation in the ENS

and to understand whether the process underlying αSyn accumulation in the gut can also lead to αSyn pathology in the brain.

Inflammation can potentially trigger αSyn pathology in the ENS of the gut and in the brain. A recent finding in children with gastrointestinal inflammation suggests an immune regulatory function of αSyn [21]. Immune pathways are indeed activated in the brain and colon of PD cases [22,23]. Also, several genes associated with an increased PD risk have an immune system-related function [24], and it was recently proposed that PD heritability is not simply due to variation in brain-specific genes, but that several cell types in different tissues are involved [25]. Adding further genetic evidence supporting that inflammation is involved in PD pathogenesis, a genome-wide association study identified common genetic pathways linking PD and autoimmune disorders [26]. Most prominently, LRRK2, a major genetic risk factor for PD also confers increased risk for developing inflammatory bowel disease (IBD) [27] and is known to modulate the function of monocytes, macrophages and other immune cells [28,29]. Intriguingly, IBD is associated with an increased risk for developing PD and specifically blocking the tumor necrosis factor (TNF) pathway reduces this risk [30–34]. Recently, it was reported that experimental colitis in αSyn transgenic mice leads to enteric accumulation of αSyn and the development of PD-like brain pathology and symptoms within a few months [35]. Converging clinical and nonclinical data suggest that the intestinal immune environment plays a role in triggering PD or facilitating the molecular events involved in the earliest phases of the disease process [36,37].

Here, we tested the hypothesis that specific types and severity of intestinal inflammation are required to trigger the accumulation of αSyn in the ENS and the subsequent development of αSyn pathology in the brain. Experimental forms of colitis in wild type and αSyn transgenic mice demonstrated that the type and degree of inflammation regulates the amount of αSyn accumulation in the colon. Macrophage-related signaling limited the extent of αSyn immunoreactivity. When αSyn transgenic mice were exposed to experimental colitis at 3 months of age and then were allowed to age normally up to 9 or 21 months, the accumulation of aggregated αSyn in midbrain, including the SN, was much exacerbated in the 21-month old group, but not in the 9-month old group. These 21-month old mice

148 also exhibited loss of nigral tyrosine hydroxylase-immunoreactive neurons. Together, our data
149 provide evidence that certain specific forms of intestinal inflammation might be a relevant upstream
150 trigger that plays a critical role in the initiation of PD pathogenesis and the disease progression.

151

152

Methods

Aim, design and setting

We aimed to combine an αSyn-transgenic mouse model of age-dependent development of αSyn pathology with well-established experimental colitis paradigms in order to explore the effect of type and severity of immune activation on the development of αSyn pathology in the colon and the brain. The design and setting of the different studies are illustrated in **Fig. 1**.

Mice

Male C57BL/6J wild type mice (Jackson Laboratories, Bar Harbor, USA), hemizygous Tg(Thy1-SNCA*A30P)18Pjk ((Thy1)-h[A30P]αSyn) [38] and Tg(Thy1-SNCA*A30P)18Pjk crossed with Cx3cr1tm1Litt ((Thy1)-h[A30P]αSyn /Cx3cr1-def; homozygous for Cx3cr1-GFP knock-in allele; [39] transgenic mice were used for the study. (Thy1)-h[A30P]αSyn transgenic mice express mutant human αSyn under the neuron selective Thy1 promoter. (Thy1)-h[A30P]αSyn transgenic mice were crossed to Cx3cr1-def transgenic mice which express eGFP replacing fractalkine receptor gene expression. All mice were maintained on a C57BL/6J background for more than 10 generations and under specific pathogen-free conditions. To the extent possible, littermates were used in the experiments. Health status was monitored daily during experiments. The in vivo experiments were endorsed by a Roche internal review board and approved by the local animal welfare authorities of the Canton Basel-Stadt, Basel, Switzerland.

Experimental colitis paradigms in mice

Paradigms for the induction of inflammation were either 1 week (acute) or 3-4 weeks (chronic) with or without an incubation phase under normal conditions of 2, 6, or 18 months post application (**Fig. 1**). Acute systemic inflammation was induced by intraperitoneal lipopolysaccharide (LPS) application [40] of 0.5 mg/kg in 100 µl injection volume on day 1 and 4 (Sigma-Aldrich Chemie GmbH, Steinheim, Germany, LPS 055:B5). Acute colitis was induced by application of 36-50kDa Dextran Sulfate Sodium (DSS) [41] (160110, MP Biomedicals, LLC, Illkirch, France) at 0%, 1%, 2.5% or 5%

180 in autoclaved drinking water for 5 continuous days respectively, followed by 2 days of water (1 DSS
181 application cycle). Chronic colitis was achieved by 4 repeating DSS application cycles. The DSS
182 concentration during 4 weeks of chronic colitis was either 1% or 2.5% for 4 weeks or 2.5%-4% raised
183 0.5% every week for 4 weeks. Mice from same littermate group were randomized per cage into
184 vehicle and inflammation inducing agent.
185
186 ***IL-10 treatment and exposure measurement***
187 Two different forms of mouse IgG bound murine IL-10 (mIgG(v1)-mIL10 and mIgG(v2)-mIL10)
188 were diluted in pre-prepared sterile formulation buffer comprised of 0.5% mouse serum supplemented
189 with 25mM citrate, 300mM arginine to a final concentration of 0.75 mg/ml and the pH adjusted to 6.7
190 on the day of application. Each mouse was treated once with 150 µg i.p. concurrently with the
191 initiation of the acute colitis paradigm with 5% DSS. The concentrations of mIgG-mIL10 fusion
192 proteins in murine serum samples were determined by enzyme-linked immunosorbent assays (ELISA)
193 specific for the Fab moiety of the administered mIgG-mIL10 fusion protein. Biotinylated mIgG-
194 mIL10-specific target molecules were used for capturing, goat anti-mIg IgG-HRP conjugate and
195 peroxidase substrate ABTS was used for quantitative detection of mIgG-mIL10 fusion proteins.
196
197 ***Immunohistochemistry***
198 Mice were injected with a lethal dose of pentobarbital (150 mg/kg). Upon full anesthesia, mice
199 received transcardial perfusion with room temperature phosphate buffered saline (PBS). For
200 biochemical and immunohistochemical analysis, one section of the proximal colon was either fresh
201 frozen and stored at -80°C or post-fixed in 4% paraformaldehyde (PFA) solution for 24 h. Following
202 post-fixation, organs were incubated in 30% sucrose/PBS at 4°C for at least 48 h before further
203 processing. Subsequently, enteric tissue was cryotome-sectioned to 35 µm thick longitudinal sections
204 (approx. 1 cm length). The brain was collected and post-fixed for 24 h in 4% PFA followed by 30%
205 sucrose in phosphate buffer until cryo-sectioning of floating sections at 40 µm. Histological analysis
206 of mouse colon was performed using standard hematoxylin staining. Immunohistochemical staining
207 was accomplished using the Vectastain Elite ABC Kits and Peroxidase Substrate Kit SK-4100 (Vector

Laboratories, Burlingame, CA, USA) or fluorescently labelled secondary antibodies (Alexa coupled to dye 488, 555 or 647, Life Technologies, Zug, Switzerland). The following primary antibodies have been used for overnight incubation at a dilution of 1:1000: monoclonal antibody to human α-synuclein (clone 211, sc-12767, Santa Cruz Biotechnology, Heidelberg, Germany), monoclonal antibody generated towards rat α-synuclein, cross-reactive with murine and human αSyn (Syn1/clone 42, BD Transduction Laboratories, Allschwil, Switzerland; used for wild type mice), polyclonal antibody to the peripheral neuronal marker Peripherin (Millipore Corporation, Billerica, MA, USA), and polyclonal antibody to macrophage marker Iba1 (Wako Chemical GmbH, Neuss, Germany). To detect phosphorylated αSyn (pSer129 pathology) in the free-floating brain sections, monoclonal antibody (ab51253, Abcam, Cambridge, USA) to human αSyn was used at a dilution of 1:10000. Prior to the pSer129 staining, the free-floating brain sections were incubated for 10 min at room temperature in a phosphate buffered saline solution containing 10 µg/mL proteinase K (Cat # 25530015; Invitrogen, California, USA). TH-immunoreactive cells were detected using a polyclonal antibody (657012, Millipore Sigma) at a dilution of 1:1000. To measure the density of Nissl-positive cells, the TH-stained cells were counter-stained with Cresyl violet. The slides were incubated in 0.1% Cresyl violet solution for 9 min and then dehydrated in 95% and 100% ethanol and then xylene prior to cover slipping with Cytoseal 60 mounting media (Thermo Fisher Scientific). Quantifications of the blind-coded TH/Nissl stained slides were done using Stereoinvestigator (version 2017.01.1; MBF Bioscience, Williams, VT, USA) on Imager M2 microscope (ZEISS) coupled to a computer. We analyzed 5-7 nigral sections per animal, and a total of 7-8 animals per treatment group. We outlined the substantia nigra pars compacta and counted every TH-immunoreactive and Nissl-positive cell in that area (using a counting frame of 40 µm x 40 µm, grid size of 140 µm x 140 µm, a guard zone of 2 µm and optical dissector height of 20 µm) and then computed the number of cells per section, generating the average cell count per animal. We then calculated the average count of cells per treatment group and analyzed the data using unpaired Student's T-test after confirming normality and homoscedasticity in Prism 7.0 (GraphPad Software).

Imaging and stereological quantification of αSyn deposits in enteric nervous system

Imaging and stereological quantification was performed on a Zeiss Axio Imager Z2 fluorescence microscope (Carl Zeiss AG, Jena, Germany). Leica TCS SP5 confocal system using an HCX PL APO CS 40x 1.3 oil UV or an HCX PL APO LB 63x 1.4 oil UV objective was utilized for image recording. Accumulation of αSyn in the ENS was assessed on a random set of 3 adjacent 35 µm thick, αSyn-immunostained sections comprising the myenteric and submucosal neuronal plexuses. Analysis was performed with the aid of Stereologer software (Stereo Investigator 10, MBF Bioscience, Williams, VT, USA) as described previously [42]. In the myenteric plexus ganglion volume was defined by multiple outlined plexuses containing a range of 5-20 neuronal cells and quantified by the optical fraction fractionator technique. In contrast to the myenteric plexus, the submucosa consists of compact plexuses with 1-5 cells including interconnecting neurites. Therefore, the entire submucosa was set as region of interest, analyzed with the area fraction fractionator technique. Results of the submucosal plexus are displayed by percent area containing αSyn deposits. For the IL-10 experiment, αSyn positive inclusions from immunofluorescence images were counted for each image. Inclusion body-like features were filtered based on having a size between 12 and 50000 pixels and a minimal intensity value greater than 300. The filtering step was included to exclude small background features and macrophages (very large spots). The counts were then aggregated to the animal level by summing the inclusion feature counts of all images per animal and then normalizing for (i.e. dividing by) the number of images for a given animal. Upon exploratory data analysis two animals were excluded: one mouse because it only had one image and another due it being an outlier, based on its infiltration score and image data.

Quantification of leukocytes infiltration

To determine the leukocyte covered area in the colon after LPS or DSS application, three adjacent hematoxylin stained sections were quantified. Total area of colon sections and localizations of leukocyte assemblies within the tissue architecture were identified and outlined utilizing Stereologer Software (Stereo Investigator 6, MBF Bioscience, Williams, VT, USA). Percentage of leukocyte covered area has been set in proportion to total area of the analyzed colon section, e.g. to at least the

length of 1 cm of proximal colon. For the IL-10 experiment, hematoxylin stained colon slices were examined by an expert pathologist blinded to treatment conditions. A score of 0-3 was assigned to each section for each of the 3 layers lamina propria, submucosa and muscularis based on the degree of inflammatory infiltration. A score of 0 denoted no inflammation and a score of 3 indicated extensive infiltration. The mean of the values for all 3 layers was taken as the final measure of leukocyte infiltration per mouse.

Quantification of αSyn/Iba1 double positive macrophages

The number of α-syn-positive Iba1 cells was evaluated by quantification of 10 random regions in 2 adjacent sections of the proximal colon. The region of interest was set to contain the myenteric plexus/circular muscle layer and the submucosal plexus. Cells were assessed for positive αSyn staining and concomitant co-localization with the macrophage marker Iba1 was quantified.

Scoring of pSer129 pathology and brain heatmap

We evaluated pSer129 pathology on a full series of immunostained coronal sections from 10 mice per treatment group (i.e. water vs. DSS-treated groups) on blind-coded slides using a previously described method [43]. We visualized pathology from one hemisphere of all brain sections (apart from the olfactory area) using NIKON Eclipse Ni-U microscope and assigned scores ranging from 0 to 4 to each brain area based on the relative abundance of PK-resistant pSer129-positive inclusions (i.e. cell bodies and neurites). In this case, 0 = no aggregates, 1 = sparse, 2 = mild, 3= dense, 4 = very dense. For the heatmap, we obtained the average score values of each brain area for each treatment group. The average data for each treatment group (n=10/ group) was then represented as a heatmap in a sagittal mouse brain background. To create the brain heatmap a postscript file downloaded freely from (http://atlas.brain-map.org/atlas?atlas=2#atlas=2&structure=771&resolution=16.75&x=7755.7470703125&y=3899.625&zoom=-3&plate=100883867&z=5) was converted to an XML in R v 3.4.4, and the mean scores were manually assigned to respective brain regions. The remaining brain regions were estimated via the R package 'Akima', using a pointwise bivariate interpolation algorithm for irregular data on the mean X and Y coordinates for each brain region.

Densitometry of pSer129 αSyn brain pathology

The density of pSer129 pathology in 12 major brain areas (reticular nucleus, pontine reticular nucleus, periaqueductal gray, gray and white layer, reticular formation, substantia nigra, ventral tegmental area, thalamus, hypothalamus, central amygdala, pallidum and striatum) was determined in the water and DSS-treated animals. A NIKON Eclipse Ni-U microscope was used to acquire 20x magnification images (without condenser lens) from all the indicated brain areas, using the same exposure time for all images. In all cases, images were acquired on three sections separated by 420 μm intervals (localized between Bregma). We then processed the acquired images using Image J64 [44], created a mask (to exclude background) that redirects to the original image for analysis, measured the total area and the mean grey value of the area that had inclusions. For brain areas such as periaqueductal gray that do not fill the entirety of the field to be analyzed, we drew a contour of the area and the analysis was performed only within that contoured area. We subsequently calculated the grey value of the area per square pixels for each image (i.e. A.U./px^2 = mean grey value x area stained/total area assessed). Based on this, we calculated the average grey value per square pixels for each brain area for each animal (n = 6 mice/group), and then extended this calculation to determine the average grey value per square pixels for each treatment group and each of the twelve brain areas of interest.

Blinding of experimenters for histological and immunohistochemical analyses

For analyses of colon and brain tissue on slides, a second individual assigned unique codes to stained slides. Therefore, the experimenter conducted the analyses blinded to the identity of the mice. For randomization of treatment groups see above.

mRNA expression

To assess mRNA expression levels from the proximal colon, RNA was extracted from fresh frozen tissue with MagnaLyser green beads (Roche Diagnostics, Mannheim, Germany) and Qiazol Lysis (Reagent cat.no.79306, Hilden, Germany) purified on MagnaPure LC (HP Kit no.03542394001, F.

Hoffmann - La Roche AG, Rotkreuz, Switzerland) and amplified via real-time PCR (4ng RNA/reaction; Lightcycler 480, Roche Diagnostics Corporation, Indianapolis, USA). Amplification of mRNA was performed by using TaqMan probes for human or murine specific α-synuclein and for selected cytokines/chemokines (Applied Biosystems Europe B.V., Zug, Switzerland). Target mRNA was normalized to tissue specific murine GAPDH levels and displayed as relative expression after 30 amplification cycles.

Statistics

Measurements for inflammation and αSyn accumulation in the ENS were taken from distinct samples (e.g. in three to six technical replicates per mouse). Data from each mouse was used only once, thus no repeated measure of same sample was performed. Statistical analysis of gut pathology and inflammation was performed using GraphPad Prism 6.04 or 7.0 software (GraphPad Software, Inc. La Jolla, CA, USA). The results are expressed as mean values ± standard errors of the mean (SEM). Student's T-test (or Welch's T-test for unequal variances) was used to compare two groups and ANOVA was used for multi-comparison of groups followed by Tukey HSD post-hoc analysis. For the statistical analysis of the mRNA expression, data quality was assessed by inspecting the distribution of Cp values of reference endogenous genes across samples, by inspecting the level of Cp variation between technical replicates and by exploring the samples multivariate signal distribution as in a principal component analysis. Relative gene expression levels were expressed as $2^{-(Cpgene - CpRef)}$. Statistical analyses to assess the effect of the experimental conditions on the log2 gene expression levels were done with linear models using the *limma* package (Bioconductor/R, [45]). These analyses were implemented in R v3.1.1.

For the statistical modelling of the effects of the IL-10 treatment on αSyn counts, as well as infiltration scores, the levels for IgG1(v1)-IL10 and IgG1(v2)-IL10 treatment were compared to the positive (vehicle/DSS) control. Additionally, since levels of the control antibody treatment (IgG1(v1)) were very similar to the positive control, the two groups were pooled in further contrasts in which effects of individual antibodies or control IgG was assessed. For αSyn counts in the enteric nervous system, a linear model on the treatment groups with one-degree freedom contrasts was applied. For

the infiltration score a Kruskal-Wallis test, with the same contrasts, was used. All statistical tests were two-tailed with a significance level of $p < 0.05$.

For the statistical analysis of the pSer129 αSyn brain pathology, zero-inflated negative-binomial mixed-effects models with a random intercept for each sample and variance assumed to increase linearly with the mean (verified against a quadratic increase using Akaike Information Criterion [AIC] and Bayesian Information Criterion [BIC]) were used to analyze the dataset via the 'glmmTMB' package in R v 3.4.4. Linear contrasts with false discovery rate (FDR) adjustments were then used to test our hypotheses and account for multiple testing (for brain area and experimental group).

Results

Experimental colitis exacerbates αSyn load in submucosal plexus of αSyn transgenic and wild type mice

During the process of further characterizing a (Thy1)-h[A30P]αSyn transgenic mouse line [38], we detected human αSyn accumulation in all innervated organs that were analyzed (**Additional File 1 Suppl. Fig. 1**). This included the myenteric and submucosal plexuses of the ENS, where human αSyn co-localized with peripherin, a specific marker for peripheral nerves (**Fig. 1a**). We observed an age-dependent increase of baseline human αSyn inclusions (irregularly sized and shaped inclusion bodies detected by human αSyn specific monoclonal antibody clone 211) in both plexuses between the ages of three and twelve months (**Fig. 1b**). We wanted to test whether IBD-related experimental inflammation in the colon exacerbates this local accumulation of αSyn acutely (e.g. within a few days or weeks) and how the age of the αSyn transgenic mice influenced the outcome. Administration of dextran sulfate sodium (DSS) in the drinking water in acute or chronic paradigms are well-established mouse models of experimental colitis mimicking aspects of IBD, i.e. by exhibiting infiltration of leukocytes into the submucosa with various degrees of destruction of the colonic mucosa and submucosa [46]. It is well known, that the DSS model can vary substantially based on the genetic background of the mice and due to different animal housing environments. Thus, in order to establish the DSS model in our environment and with our mice, we first tested DSS administration at different concentrations and durations in the (Thy1)-h[A30P]αSyn transgenic mice (**Fig. 1c**), and observed leukocyte infiltration in a dose-dependent manner, which was similar at the age of 3 and 6 months (**Fig. 1d and 2a**). In the acute paradigm with mice at the age of 3 months, 2.5%, but not 1%, DSS triggered intracellular accumulation of αSyn in nerves of the submucosal plexus **(Fig. 2a, b)**. In the chronic DSS paradigm, which was initiated in the mice at the age of 3 months (and terminated when they were 6 months old; these animals were allowed to age to 6 months following the one month chronic treatment; **Fig. 1c and 2c**), we observed a dose-dependent increase of αSyn load in the submucosal plexus, but at a smaller magnitude than in the younger mouse cohort **(Fig. 2a)**. In that context, it was also interesting to observe that (Thy1)-h[A30P]αSyn transgenic mice exposed to acute

DSS colitis presented with several αSyn-positive cells with a morphology consistent with them being infiltrating leucocytes, which we confirmed to be positive for the macrophage marker Iba-1 (**Suppl. Fig. 2**). This finding was relevant for the quantification of αSyn inclusions in the myenteric and submucosal plexus; i.e. such features were excluded from the quantification process.

Wild type mice also express endogenous αSyn in innervated organs, but at much lower levels compared with human αSyn protein that was overexpressed by the hemizygous (Thy1)-h[A30P]αSyn transgenic mice (**Suppl. Fig. 1**). To confirm that the finding in (Thy1)-h[A30P]αSyn transgenic mice was independent of transgenic expression of human αSyn, we applied the acute and the constant dose chronic DSS paradigms also in wild type mice (**Fig. 1c**). In both treatment paradigms, we observed in the submucosal plexus small inclusion bodies of endogenous murine αSyn (detected by rodent cross-reactive αSyn-specific monoclonal antibody Syn1/clone 42, **Fig. 2c, d**). These features were close to undetectable in the water group that did not experience experimental colitis. A separate experiment also confirmed that the observed effects of DSS could not be attributed to increased gene expression of murine or the transgenic human αSyn **(Suppl. Fig. 3)**. Together, these results confirmed the validity of this experimental IBD paradigm to test the effect of inflammation on αSyn accumulation in the ENS in wild type and (Thy1)-h[A30P]αSyn transgenic mice. Because 3-month old (Thy1)-h[A30P]αSyn transgenic mice provided more optimal conditions for visualization and quantification of αSyn inclusions in the ENS, for the remainder of the study we focused on using this transgenic mouse model.

Colitis induced by peroral DSS but not by peritoneal administration of LPS aggravates αSyn accumulation in colonic submucosal plexus of αSyn transgenic mice

In order to explore the effects of different approaches to induce inflammation in or nearby the gut in (Thy1)-h[A30P]αSyn transgenic mice, we compared the outcome of acute 5% DSS in drinking water with acute 0.5 mg/kg intraperitoneal LPS administration (**Fig. 1c and 3**). To maximize the inflammatory response, we administered both DSS and LPS at relatively high doses. At day 7, both agents had induced variable degrees of leukocyte infiltration in the submucosa of the colon while a marked destruction of the mucosa was induced when giving only DSS (**Fig. 1d**). As before, the DSS-

exposed mice presented with increased accumulation of αSyn in the ganglia of the submucosal plexus (**Fig. 3a**). In contrast, we detected no change in αSyn load in the myenteric plexus, consistent with lack of leukocyte infiltration in this part of the colonic wall (**Fig. 3b**). Despite the high dose, LPS-induced inflammation did not increase αSyn accumulation in the colonic nervous plexuses (**Fig. 3c, d**). Notably, LPS and DSS resulted in a differential expression of cytokines, and consistent with leukocyte recruitment, CCL2 was elevated in both (**Fig. 3f, g**). In the LPS paradigm, mRNA for IL-10 was markedly elevated, whereas DSS strongly increased IL-6 and also IL-1β but not IL-10. Together these results indicate that, in our model, colonic inflammation induced by peroral DSS but not intraperitoneal LPS increases the accumulation of αSyn in the colon.

Lack of Cx3cr1 signaling during DSS colitis aggravates αSyn load in the submucosal plexus of αSyn transgenic mice

Given the role of monocytes/macrophages in IBD and in the related DSS paradigm, we hypothesized further that modulating monocytes/macrophages may affect accumulation of αSyn in our DSS model as well. In a first set of experiments we manipulated monocytes/macrophages genetically by crossing (Thy1)-h[A30P]αSyn transgenic mice with mice that have a deletion for the fractalkine receptor Cx3cr1 (Cx3cr1-GFP knock-in mice) (**Fig. 3a, b**). The CX3CR1-CX3CL1 axis plays an important role in maintaining the function of the lamina propria macrophage population of the gastrointestinal wall and lack of this signaling pathway in experimental colitis models may either aggravate or ameliorate the induced pathology [47–49]. In our experiment, the area covered by infiltrating leukocytes following exposure to DSS was near the mucosa and submucosa and was not significantly higher in the Cx3cr1-deficient αSyn transgenic mice than in the Cx3cr1-competent mice (**Suppl. Fig. 3a**). However, a significantly higher level of αSyn accumulated in the submucosal plexus in αSyn transgenic mice lacking Cx3cr1 compared to αSyn transgenic mice expressing Cx3cr1 ($p = 0.001$, two-way ANOVA with Tukey HSD post-hoc analysis; **Fig. 3a**). In the myenteric plexus, we found no marked increase in αSyn accumulation in neither the αSyn transgenic mice with normal Cx3cr1 nor the αSyn transgenic mice deficient in Cx3cr1, indicating as in the experiments above a possible prominent role for the localization of leukocyte infiltration in the process of αSyn accumulation in the

submucosa **(Fig. 3b)**. Collectively, our results in Cx3cr1-deficent αSyn transgenic mice provide a potential association between monocyte/macrophage signaling and αSyn accumulation in ENS in this experimental IBD model.

Systemic IL-10 ameliorates DSS-induced colitis and associated enteric αSyn accumulation in αSyn transgenic mice

To continue testing the hypothesis that modulating monocytes/macrophages may affect accumulation of αSyn in our DSS model we moved to a pharmacological modulation of this cellular subset. Interleukin-10 (IL-10) is an important regulator of monocytes/macrophages, and genetic ablation of IL-10 signaling or blocking IL-10 with specific antibodies has been reported to enhance DSS colitis [50,51]. In the experiments with LPS we had also noted an increase of IL-10 compared with the DSS paradigm and LPS inflammation was in contrast to DSS colitis not associated with increased αSyn accumulation in the ENS (**Fig. 3**). To mimic the effect of higher levels of IL-10 in an acute model of DSS colitis (5% DSS, **Fig. 1c**), we administered intravenously recombinant murine IL-10 (mIL10). The half-life of injected recombinant IL-10 protein in blood is very short. To reduce the number of injections, we extended the half-life of mIL-10 in circulation by engineering it onto two different murine IgG variants (i.e., mIgG1(v1)-mIL10 and mIgG1(v2)-mIL10, respectively). As described above, DSS induced a marked increase in leukocyte infiltration and αSyn accumulation, and we found both to be similar in the untreated and control IgG treated group (**Fig. 4a, b**). In contrast, both mIgG1(v1)-mIL10 and mIgG1(v2)-mIL10 significantly reduced leukocyte infiltration in mice treated with DSS ($p<0.0001$, one-way ANOVA with Tukey HSD post-hoc analysis; **Fig. 4a, b**). A significant down-regulatory effect of an IL-10 treatment on DSS colitis induced accumulation of human αSyn in the submucosal plexus was only observed with mIgG1(v2)-mIL10 ($p=0.02$, one-way ANOVA with Tukey HSD post-hoc analysis; **Fig. 4b**). This effect by mIgG1(v2)-mIL10 on αSyn levels was accompanied by detectable serum levels of mIgG1(v2)-mIL10 at the end of the *in vivo* phase, whereas mIgG1(v1)-mIL10 was no longer detectable at that point (**Fig. 4c**). This indicates that although both forms of IL-10 have a down-regulatory effect on leukocyte infiltration, a sustained pharmacological exposure of IL-10 may be required for reducing αSyn accumulation. These results highlight an

important role for the IL-10 pathway in keeping αSyn accumulation at a reduced level throughout the course of experimental IBD. Together, our observations by genetic (i.e. CX3CR1-CX3CL1 axis) and pharmacological modulation (i.e. IL-10) of DSS colitis corroborate an important role for monocyte/macrophage pathways in the development of αSyn accumulation in the ENS of the colon.

DSS colitis-induced submucosal αSyn accumulation at a young age persists for months and is exacerbated by lack of Cx3cr1 signaling

In humans there is strong epidemiological evidence that IBD increases PD risk [30,32,34] and recent evidence in Crohn's disease [52] indicate that such gut inflammatory conditions are associated with αSyn accumulation in the ENS [33]. In mice we have until here established and replicated in different setups a link between modulation of inflammation and induction of αSyn accumulation in the ENS. Because longer exposure to DSS mimics more closely the chronic nature of IBD, we elected to explore αSyn accumulation in the submucosal plexus of (Thy1)-h[A30P]αSyn transgenic mice that were subjected to DSS colitis in a 4-week chronic increasing dose paradigm. In order to allow for a full recovery from the chronic inflammation, we aged the mice for two months on normal drinking water and analyzed them at the age of 6 months (**Fig. 1c**). At this point we wanted again to explore the effect of modulating monocytes/macrophages in this chronic setting and added an experimental arm with (Thy1)-h[A30P]αSyn transgenic mice lacking Cx3cr1. As expected, after 2 months of recovery, the area that is usually extensively covered by leukocytes in the submucosal plexus of the acute DSS paradigm had returned to normal levels following the two-month recovery period (**Suppl. Fig. 4a**). Remarkably, however, αSyn accumulation in the ganglia of the submucosal plexus was still almost doubled when compared to αSyn transgenic mice that were not exposed to DSS, and this was exacerbated in αSyn transgenic mice deficient for Cx3cr1 (**Suppl. Fig. 4b**). The finding in the αSyn transgenic mice suggests that accumulation of αSyn is not a transient effect or response. In addition, modulation of monocytes/macrophages by down-regulating the CX3CR1-CX3CL1 axis contributes to aggravation of this accumulation.

494 ***Experimental colitis-induced at a young age exacerbates αSyn brain pathology and dopaminergic***
495 ***neuron loss in old αSyn transgenic mice***
496 At this point, we have established and repeatedly demonstrated that modulation of inflammatory
497 mechanisms in experimental colitis induced by acute and chronic DSS administration is causatively
498 linked to induction and persistence of αSyn accumulation in the ENS of young adult mice. The
499 previously highlighted hypothesis by Braak and colleagues associates αSyn brain pathology in PD
500 with αSyn pathology in the ENS earlier in life [3,53]. To assess development of brain αSyn pathology
501 and to link it again to IBD risk, we exposed 3-month old hemizygous (Thy1)-h[A30P]αSyn transgenic
502 mice to DSS or normal drinking water and after 23 days on this chronic increasing dose paradigm
503 returned all mice to normal drinking water until sacrifice (**Fig. 1c, increasing dose**). We chose to use
504 the αSyn transgenic model rather than wild type mice for this study because of two reasons: 1) we
505 knew that the model as hemizygous transgenic mice exhibit some αSyn brain pathology that develops
506 slowly under baseline conditions. Importantly, the pathology is much less pronounced than in
507 homozygous (Thy1)-h[A30P]αSyn mice [54]; 2) at the time of the experiment, it was not clear
508 whether wild type mice could develop αSyn brain pathology upon DSS colitis. Thus, we chose
509 hemizygous (Thy1)-h[A30P]αSyn transgenic mice to increase the chances for a successful outcome
510 and potentially to aggravate the brain pathology from mild to strong. After exposing the mice either to
511 normal drinking water or a chronic DSS paradigm, we aged them in two cohorts on normal water and
512 housing conditions to either up to the age of 9 months (cohort 1) or 21 months (cohort 2). At these
513 two timepoints we analyzed various brain regions for pathological αSyn (proteinase K resistant,
514 pSer129-αSyn immunoreactive inclusions). When we examined the αSyn transgenic mice of cohort 1,
515 we found that both experimental groups (i.e. those who were on DSS and those who stayed on normal
516 water throughout their entire life and thus never experienced DSS colitis) exhibited extremely low
517 levels of pathological αSyn inclusions in the brain (**Fig. 5A-F, M-Q and Suppl. Fig. 5a**). Our
518 observation of the level of pathological αSyn inclusions in the brain of these 9-month old hemizygous
519 (Thy1)-h[A30P]αSyn transgenic mice is indeed consistent with earlier descriptions of the model at the
520 age of 11 months [54]. Similarly for cohort 2, the 21-month old hemizygous (Thy1)-h[A30P]αSyn
521 transgenic mice that only received water during their lifetimes showed relatively low levels of

pathological αSyn in the brain (**Fig. 5G-I and Suppl. Fig. 5b**), which is consistent with previous observations in this transgenic line at the age of 24 months [54]. In marked contrast, the 21-month-old hemizygous (Thy1)-h[A30P]αSyn transgenic mice that were exposed to DSS at three months of age presented with pSer129-positive αSyn pathology throughout various brain regions in a much more exacerbated fashion than mice that were aged up to 21 months without having experienced DSS colitis at young age (**Fig. 5J-L, R-V and Suppl. Fig. 5c**). The degree and distribution of proteinase K resistant αSyn was similar to what was previously described for homozygous (Thy1)-h[A30P]αSyn transgenic mice at the age of 8 to 9 months [54]. The significant aggravation of αSyn pathology in the substantia nigra ($p \leq 0.01$ in a negative-binomial mixed-effects model adjusting for multiple comparisons performed over all brain areas) was accompanied by a significant loss of tyrosine hydroxylase (TH) and Nissl-positive cells at 21 months of age ($p \leq 0.05$, Student's T-test; **Fig. 6**). Together, we found that experimental DSS colitis at a young age caused an age-dependent exacerbation of αSyn inclusion pathology and a loss of nigral dopaminergic neurons in the brains of (Thy1)-h[A30P]αSyn transgenic mice.

Discussion

Currently, there is no therapy for PD available to slow or stop disease progression and an obstacle in the quest to develop one is that we do not understand how the disease develops [55]. Intraneuronal accumulation of αSyn (i.e. in Lewy bodies and neurites) is a key neuropathological hallmark and the distribution of Lewy pathology in postmortem brain is used for staging in PD [2,56]. Accumulation of αSyn has also been observed in the peripheral nervous system in PD, some individuals at risk of developing the disease, and normal individuals [57–59]. Similar to this finding in people, αSyn-immunoreactive inclusions have also been detected in the ENS of a transgenic mouse model prior to changes in the brain [60]. Based on preclinical models employing injection of recombinant αSyn fibrils to different brain regions and intestines [15,16,19,20,43,61,62] together with postmortem brain pathology [53,56,63], it has also been suggested that αSyn pathology propagates temporospatially

549 from cell-to-cell in a prion-like manner [3,56,61,63,64]. However, the initial factors triggering αSyn
550 aggregation are yet to be established [55] and the involvement of peripheral stimuli in the aggregation
551 and pathogenic spread of αSyn is only beginning to unravel.

552 In this study, we provide evidence that DSS colitis, i.e. an experimental IBD-like inflammation,
553 triggers αSyn accumulation in the ENS of wild type mice and in a transgenic mouse model of PD
554 (**Fig. 2**). We found aggravation of enteric αSyn accumulation in αSyn transgenic mice lacking Cx3cr1
555 signaling and amelioration of inflammation and enteric αSyn load by systemic IL-10, demonstrating
556 that genetic and pharmacologic modulation of inflammation can influence the degree of αSyn
557 accumulation in the ENS (**Fig. 3 and 4**). The capability of IL-10 and the CX3CR1-CX3CL1 axis
558 being able to mediate this effect suggests that monocytes/macrophages modulate the process in this
559 model. We further observed that the aggravated αSyn accumulation in the ENS persisted even after
560 two months of recovery from DSS colitis and was aggravated in the absence of CX3CR1 signaling.
561 This indicates that the effect is not transient and further establishes that monocytes/macrophages play
562 a critical role in this process (**Suppl. Fig. 4**). Remarkably, at 18 months but not 6 months post
563 induction of DSS colitis (thus, at age 21 months but not 9 months, respectively), αSyn transgenic mice
564 had developed massively elevated αSyn brain pathology (**Fig. 5 and Suppl. Fig. 5**). This elevated
565 proteinase K resistant pSer129-αSyn pathology in the midbrain, including the substantia nigra, and
566 other brain regions coincided with an average decrease of 30-50% of TH- and Nissl-positive cells in
567 the nigra (**Fig. 6**). We chose to perform the long-term experiments in αSyn transgenic mice rather than
568 wild type mice. These particular αSyn transgenic mice had previously been shown to slowly develop
569 αSyn pathology in the brain on a homozygous genotype [38,54] making them ideal when asking the
570 question of whether transient colonic inflammation can aggravate brain pathology in a genetically
571 predisposed animal such as the hemizygous transgenic mice used in this study. Others have recently
572 demonstrated in a more aggressive αSyn transgenic mouse model that mild DSS colitis can accelerate
573 αSyn accumulation in the ENS and brain [35]. In future long-term studies, we plan to address whether
574 αSyn pathology develops also in the brains of wild type mice if they sustain transient experimental
575 IBD at a young age. In our experiments presented here, experimental DSS colitis in αSyn transgenic

mice recapitulated the accumulation of enteric αSyn which is proposed to occur in humans several years before PD diagnosis [36]. Additionally, the subsequent age-related development of αSyn pathology in the brain of αSyn transgenic mice together with the loss of nigral dopaminergic neurons mimicked a progression of the disease similar to what is considered to occur in PD.

We established that a mechanism by which a specific type of peripheral inflammation promotes αSyn accumulation in the colon potentially involves monocytes and macrophages. Both peroral DSS and intraperitoneal LPS administration provoked strong local immune reactions resulting in leukocyte infiltration into the submucosa of the colon. The region of the colon which was inflamed contains the submucosal plexus and is anatomically separated from the myenteric plexus by a thick circular muscle (**Fig. 1**). This discrete localization of inflammation to the submucosa might explain why αSyn only accumulated in the nerves of the submucosal plexus and not in the myenteric plexus of our mice that received DSS in both a strong acute and the two chronic paradigms. The mechanism underlying how intraperitoneally administered LPS leads to submucosal leukocyte infiltration likely involves the monocyte attractant chemokine CCL2 (**Fig. 3**), but the specifics remain to be clarified [65]. Indeed, CCL2 was also upregulated in the colon of our DSS model. However, in contrast to intraperitoneal LPS, where infiltrating macrophages were present in discrete patches in the colonic wall, DSS-related macrophage infiltration was distributed both in small groups and larger randomly distributed patches of cells across the entire colonic submucosa. Also, perorally administered DSS destroys the mucosa of the colon, similar to some forms of ulcerative colitis, resulting in the transient disintegration of the intestinal epithelial barrier. In our (Thy1)-h[A30P]αSyn transgenic mice, the subsequent immune response to the infiltration of commensal bacteria evoked an elevated expression of cytokines such as IL-1β and IL-6, a phenomenon also observed in in the colon of IBD patients [66,67]. This upregulation was absent in the LPS paradigm in which the intestinal mucosa remained intact. By acting on tight junctions, IL-1β and IL-6 can increase intestinal barrier permeability (gut leakiness), facilitating the recruitment of additional immune cells to the site of the inflammation, eventually culminating in widespread immune activation [68,69]. Consistent with the breach of barrier permeability in our mouse model, some PD patients exhibit increased colonic cytokines such as IL-

603 1β, IL-6 and TNF, occurring together with increased intestinal permeability [22,70]. In this context, it
604 is also notable that people with Crohn's disease present with increased enteric αSyn expression [52]
605 and even more striking that IBD patients on anti-TNF therapy have a reduced risk of developing PD
606 compared to IBD patients not given this treatment [32]. Notably, mucosal macrophages with
607 intralysosomal αSyn content were previously described in the intact human appendix [71]. These
608 macrophages were in close proximity to the axonal varicosities of the vermiform appendix, which
609 showed an enriched staining for αSyn in the mucosal plexus. Furthermore, we recently found that the
610 vermiform appendix contains aggregated and truncated αSyn that has the propensity to seed
611 aggregation of recombinant αSyn *in vitro* [59].

612 What could be a functional role of the αSyn species found in abundance in the gut wall? Monomeric
613 and oligomeric αSyn species reportedly act as chemoattractants for neutrophils and monocytes,
614 enhancing the maturation of dendritic cells in the ENS [21,72]. With such a role in intestinal
615 immunity, it is possible that the tissue destruction induced by DSS in the present study led to release
616 of αSyn, which perhaps served as a chemoattractant for monocytes. The increased abundance of αSyn
617 and altered intestinal permeability, along with the DSS-evoked inflammatory response may have
618 provided an enabling milieu allowing further αSyn accumulation in the ENS of the colon [73].
619 Macrophages and other immune cells are also regulated by several genes including *LRRK2*, an
620 established risk gene for PD and IBD. It will be interesting to explore how mutations in genes that
621 control autophagy, including the *LRRK2* gene, influence the handling of αSyn by macrophages that
622 invade the inflamed colon in our DSS colitis paradigm. Despite the intriguing translational aspect of
623 our finding in the DSS paradigm, others have very recently reported that DSS colitis in mice down-
624 regulates the expression of enteric αSyn on protein levels *in vivo* [74,75]. This is in contrast to our
625 immunofluorescence (i.e. increased accumulation of αSyn in submucosal plexus upon DSS colitis;
626 **Fig. 2, 3, 4 and 5**) and gene expression data (e.g., no change in endogenous and transgenic αSyn upon
627 DSS colitis; **Suppl. Fig. 3**) in the same paradigm and may reflect the well-known lab-to-lab
628 variability that can occur for the DSS models [76].

Perhaps the most striking finding in our study was that a single period of DSS-induced colitis at a young age led to an exacerbation of αSyn pathology in the brain of αSyn transgenic mice much later in life (**Fig. 6**). How does severe αSyn inclusion pathology develop in the brains of these mice? One hypothesis is that the brain αSyn pathology observed in this study could be due to direct effects of peripheral immune activation on the brain and that certain peripheral triggers can directly affect microglial activity. For instance, short-chain fatty acids derived from gut microbiota appear to influence function and maturation of microglia in the mouse brain [77] and inflammatory mediators released by gut microbiota into the bloodstream have been suggested to induce brain pathology and behavioral changes in an αSyn transgenic mouse model [78]. Moreover, rats and nematodes have been reported to develop αSyn inclusions after exposure to the bacterial amyloid protein curli, a protein which stimulates microgliosis, astrogliosis, and secretion of IL-6 and TNF [79]. Intriguingly, a recent study reported that peripherally applied inflammatory stimuli induce acute immune training (that exacerbates β-amyloid pathology) and immune tolerance in the brain that reprograms microglia, an effect which can persist for at least six months [80]. Whether this is a relevant mechanism in the DSS paradigm needs to be explored.

Another hypothesis is that the observed brain αSyn pathology may have accumulated as a consequence of the transfer of pathogenic αSyn seeds from the gut via the vagal nerve. Several experimental studies have demonstrated that pathogenic αSyn seeds can be transferred from the peripheral to the central nervous system. Aggregated recombinant αSyn injected intraperitoneally, intramuscularly or into the gastric wall of certain mouse models of PD results in αSyn inclusions in the brain [16,81]. Data from animals injected with recombinant αSyn protein in the gut wall or viral vectors expressing αSyn into the vagal nerve suggest that pathogenic seeds can be transmitted via the vagal nerve [15,19,20,62,82–84]. A role for the vagal nerve in PD was also suggested by an epidemiological study indicating that vagotomy in a Danish population is associated with decreased PD risk [85], although this association has been challenged [86]. In the present study, αSyn pathology was much more prominent in the reticular nucleus (including the vagal nucleus) and midbrain areas compared to the rostral areas at 18 months post DSS colitis. Although we did not conduct the

definitive experiment of cutting the vagal nerve, our data are consistent with the growing body of evidence that the vagal nerve is involved in the accumulation of αSyn aggregates in the brain. That said, the innervation of the colon occurs via both parasympathetic (e.g., vagal output neurons) and sympathetic (e.g., in the celiac ganglion of the upper abdomen) nerves. The possibility of propagation of αSyn pathology via the two routes is supported by the observation that injection of recombinant αSyn fibrils to the duodenum of certain αSyn transgenic rats leads to accumulation of pathological αSyn in organs innervated by the parasympathetic and the sympathetic nerves [62] and that αSyn accumulation present in both peripheral nervous structures in humans as well [87]. Thus, propagation may occur through both vagal and spinal routes.

Conclusion

We report that αSyn accumulates in the colon of αSyn transgenic and wildtype mice subjected to experimental DSS colitis and that this process can be modulated by modifying genetically and pharmacologically pathways related to monocyte/macrophage signaling. We further demonstrate that chronic but transient DSS colitis in young αSyn transgenic mice leads to a markedly exacerbated accumulation of αSyn aggregates in the brain when the mice age. In the same aged mice, the numbers of TH- and Nissl-positive neurons in the substantia nigra are reduced, suggestive of a neurodegenerative process. Together, our findings are in consonance with studies demonstrating a link between IBD and PD [30,32,88] and suggest a critical role for specific types of intestinal inflammation and αSyn accumulation in the initiation and progression of PD.

List of abbreviations

CCL2: Chemokine (C-C motif) ligand 2; CD: Crohn's disease; CX3CR1: CX3C Chemokine receptor 1 (fractalkine receptor); DSS: Dextran Sulfate Sodium; ELISA: Enzyme-linked immunosorbent assays; ENS: Enteric nervous system; FDR: False discovery rate; IBD: Inflammatory bowel disorder;

IL: Interleukin; LPS: Lipopolysaccharide; PBS: Phosphate buffered saline; PD: Parkinson's disease; PFA: Paraformaldehyde; PK: Proteinase K; pSer129: α-synuclein phosphorylated at serine 129; SEM: Standard error of the mean; SN: Substantia nigra; TH: Tyrosine hydroxylase; TNF: Tumor necrosis factor; UC: Ulcerative colitis; αSyn: α-Synuclein.

Declarations

Ethics approval and consent to participate

The in vivo experiments were endorsed by a Roche internal review board and approved by the local animal welfare authorities of the Canton Basel-Stadt, Basel, Switzerland.

Consent for publication

Not applicable

Availability of data and materials

The datasets used and/or analyzed in this study are available from the corresponding author on reasonable request.

Competing interest

At the time of the study S.G. and N.M. were Roche Postdoctoral Fellows employed by Roche and L.S., F.B., G.D.P., J.S.P., K.O.S., H.R., M.H., M.Se. M.St., P.M., A.W., T.E., A.H. and M.B. are or were fulltime employees or trainees at Roche and they may additionally hold Roche stock/stock options. S.G. and L.S. are currently employees of Neurimmune AG, Schlieren, Switzerland. P.B. has received commercial support as a consultant from Renovo Neural, Inc., AbbVie, Neuroderm, Fujifilm-Cellular Dynamics International, Axial Biotherapeutics, and IOS Press Partners. He has received commercial support for grants/research from Lundbeck A/S, Renovo, and Roche. He has

ownership interests in Acousort AB and Axial Biotherapeutics and is on the steering committee of the NILO-PD trial. The other authors declare that they have no competing interest with regard to this research.

Funding

P.B. reports grants from the National Institutes of Health (1R01DC016519-01, 5R21NS093993-02, 1R21NS106078-01A1) and Office of the Assistant Secretary of Defense for Health Affairs (Parkinson's Research Program, Award No. W81XWH-17-1-0534). S.G and N.M. were supported by a grant from Roche under the Roche Postdoctoral Fellowship (RPF) Program.

Authors' contributions

S.G., N.M. and L.S. planned and performed the in vivo experiments, colon immunostaining, analysis, and quantification; S.G. and N.M. drafted a first version of the manuscript; E.Q. performed, imaged, quantitated pSer129, TH and Nissl staining in the brain sections, and drafted a more advanced version of the manuscript with J.A.S., who also provided helpful discussion. F.B. and K.O.S. supported the image acquisition and image analysis for the colon samples; M.St. performed imaging and data analysis of experiments with wildtype mice; G.D.P. and J.S.P. performed statistical analysis of the DSS experiments; H.R. and M.H. performed mRNA analyses; M.Se. trained S.G. and L.S. on mouse necropsy and supported their work; P.M. performed expert pathology staging on leukocyte infiltration; T.E. and A.W. provided mIgG-mIL-10 fusion proteins and measured serum exposure; Z.M. performed statistical analysis for the pSer129 αSyn immunohistochemistry data. A.S. contributed with scientific and veterinary expert input for implementation and analysis of the DSS colitis model at Roche. M.L.E.G. provided helpful discussion and project planning. A.H. co-mentored S.G. and N.M., performed expert pathology staging on leukocyte infiltration and contributed to experimental planning. C.M. trained S.G. on the colitis model and provided expert input on the experimental IBD model. M.B. and P.B. co-mentored Roche Postdoctoral Fellows S.G. and N.M., conceived and oversaw the study, and performed experimental planning; M.B., P.B. and E.Q. wrote the final version of the manuscript. All authors read and approved the final manuscript.

Acknowledgments

We thank Drs. L. Ozmen and A. Bergadano for their tremendous support in maintaining the mouse colony and we are grateful to the animal caretakers, veterinarians and many unnamed staff at Roche for their valuable work with the mice in this study. In addition, at Roche we thank Dr. K.G. Lassen for critical input to the paper, Dr. C. Ullmer for co-mentoring S.G. and providing scientific input, Dr. L. Collin for helping with confocal imaging and we are grateful to Dr. T. Kremer, N. Haenggi, D. Mona, A. Girardeau, and J. Messer for providing support in tissue dissections and G. Walker and R. Lauria for technical support. Ms. E. Schulz from VARI assisted with immunostaining of the brain tissue. We thank the Contract Research Organization Frimorfo for carefully sectioning the brains for this study. We acknowledge Drs. L. Gaudimier (née Chicha) and F. Pan-Montojo for scientific discussions early in the project, Dr. W. Zago from Prothena for valuable scientific input throughout the project, and Drs. M. and P. Derkinderen for critical input on the link between IBD and the enteric αSyn accumulation in humans.

References

1. Tysnes O-B, Storstein A. Epidemiology of Parkinson's disease. J Neural Transm (Vienna). 2017;124:901–5.

2. Spillantini MG, Goedert M. Neurodegeneration and the ordered assembly of α-synuclein. Cell Tissue Res. 2017;373:137–48.

3. Del Tredici K, Braak H. Lewy pathology and neurodegeneration in premotor Parkinson's disease. Mov Disord. 2012;27:597–607.

4. Polymeropoulos MH, Lavedan C, Leroy E, Ide SE, Dehejia A, Dutra A, et al. Mutation in the alpha-synuclein gene identified in families with Parkinson's disease. Science. 1997;276:2045–7.

5. Schrag A, Horsfall L, Walters K, Noyce A, Petersen I. Prediagnostic presentations of Parkinson's disease in primary care: a case-control study. Lancet Neurol. 2015;14:57–64.

6. Gaenslen A, Swid I, Liepelt-Scarfone I, Godau J, Berg D. The patients' perception of prodromal symptoms before the initial diagnosis of Parkinson's disease. Mov Disord. 2011;26:653–8.

7. Pont-Sunyer C, Hotter A, Gaig C, Seppi K, Compta Y, Katzenschlager R, et al. The onset of nonmotor symptoms in Parkinson's disease (the ONSET PD study). Mov Disord. 2015;30:229–37.

8. Berg D, Godau J, Seppi K, Behnke S, Liepelt-Scarfone I, Lerche S, et al. The PRIPS study: screening battery for subjects at risk for Parkinson's disease. Eur J Neurol. 2013;20:102–8.

9. Postuma RB, Gagnon J-F, Bertrand J-A, Génier Marchand D, Montplaisir JY. Parkinson risk in idiopathic REM sleep behavior disorder: preparing for neuroprotective trials. Neurology. 2015;84:1104–13.

10. Abbott RD, Petrovitch H, White LR, Masaki KH, Tanner CM, Curb JD, et al. Frequency of bowel movements and the future risk of Parkinson's disease. Neurology. 2001;57:456–62.

11. Savica R, Carlin JM, Grossardt BR, Bower JH, Ahlskog JE, Maraganore DM, et al. Medical records documentation of constipation preceding Parkinson disease: A case-control study. Neurology. 2009;73:1752–8.

12. Mahlknecht P, Seppi K, Poewe W. The Concept of Prodromal Parkinson's Disease. J Parkinsons Dis. 5:681–97.

13. Braak H, de Vos RAI, Bohl J, Del Tredici K. Gastric alpha-synuclein immunoreactive inclusions in Meissner's and Auerbach's plexuses in cases staged for Parkinson's disease-related brain pathology. Neurosci Lett. 2006;396:67–72.

14. Phillips RJ, Walter GC, Wilder SL, Baronowsky EA, Powley TL. Alpha-synuclein-immunopositive myenteric neurons and vagal preganglionic terminals: autonomic pathway implicated in Parkinson's disease? Neuroscience. 2008;153:733–50.

15. Holmqvist S, Chutna O, Bousset L, Aldrin-Kirk P, Li W, Björklund T, et al. Direct evidence of Parkinson pathology spread from the gastrointestinal tract to the brain in rats. Acta Neuropathol. 2014;128:805–20.

16. Breid S, Bernis ME, Babila JT, Garza MC, Wille H, Tamgüney G. Neuroinvasion of α-Synuclein Prionoids after Intraperitoneal and Intraglossal Inoculation. J Virol. 2016;90:9182–93.

17. Sargent D, Verchère J, Lazizzera C, Gaillard D, Lakhdar L, Streichenberger N, et al. “Prion-like” propagation of the synucleinopathy of M83 transgenic mice depends on the mouse genotype and type of inoculum. J Neurochem. 2017;143:126–35.

18. Manfredsson FP, Luk KC, Benskey MJ, Gezer A, Garcia J, Kuhn NC, et al. Induction of alpha-synuclein pathology in the enteric nervous system of the rat and non-human primate results in gastrointestinal dysmotility and transient CNS pathology. Neurobiol Dis. 2018;112:106–18.

19. Arotcarena M-L, Dovero S, Prigent A, Bourdenx M, Camus S, Porras G, et al. Bidirectional gut-to-brain and brain-to-gut propagation of synucleinopathy in non-human primates. Brain. Oxford Academic; 2020;143:1462–75.

20. Challis C, Hori A, Sampson TR, Yoo BB, Challis RC, Hamilton AM, et al. Gut-seeded α-synuclein fibrils promote gut dysfunction and brain pathology specifically in aged mice. Nature Neuroscience. Nature Publishing Group; 2020;23:327–36.

21. Stolzenberg E, Berry D, Yang D, Lee EY, Kroemer A, Kaufman S, et al. A Role for Neuronal Alpha-Synuclein in Gastrointestinal Immunity. JIN. 2017;9:456–63.

22. Devos D, Lebouvier T, Lardeux B, Biraud M, Rouaud T, Pouclet H, et al. Colonic inflammation in Parkinson’s disease. Neurobiol Dis. 2013;50:42–8.

23. Mogi M, Harada M, Kondo T, Riederer P, Inagaki H, Minami M, et al. Interleukin-1 beta, interleukin-6, epidermal growth factor and transforming growth factor-alpha are elevated in the brain from parkinsonian patients. Neurosci Lett. 1994;180:147–50.

24. Brás J, Guerreiro R, Hardy J. SnapShot: Genetics of Parkinson’s disease. Cell. 2015;160:570-570.e1.

25. Reynolds RH, Botía J, Nalls MA, Hardy J, Taliun SAG, Ryten M. Moving beyond neurons: the role of cell type-specific gene regulation in Parkinson’s disease heritability. npj Parkinson’s Disease. 2019;5:6.

26. Witoelar A, Jansen IE, Wang Y, Desikan RS, Gibbs JR, Blauwendraat C, et al. Genome-wide Pleiotropy Between Parkinson Disease and Autoimmune Diseases. JAMA Neurol. 2017;74:780–92.

27. Umeno J, Asano K, Matsushita T, Matsumoto T, Kiyohara Y, Iida M, et al. Meta-analysis of published studies identified eight additional common susceptibility loci for Crohn’s disease and ulcerative colitis. Inflamm Bowel Dis. 2011;17:2407–15.

28. Gardet A, Benita Y, Li C, Sands BE, Ballester I, Stevens C, et al. LRRK2 is involved in the IFN-gamma response and host response to pathogens. J Immunol. 2010;185:5577–85.

29. Hakimi M, Selvanantham T, Swinton E, Padmore RF, Tong Y, Kabbach G, et al. Parkinson’s disease-linked LRRK2 is expressed in circulating and tissue immune cells and upregulated following recognition of microbial structures. J Neural Transm (Vienna). 2011;118:795–808.

30. Lin J-C, Lin C-S, Hsu C-W, Lin C-L, Kao C-H. Association Between Parkinson’s Disease and Inflammatory Bowel Disease: a Nationwide Taiwanese Retrospective Cohort Study. Inflamm Bowel Dis. 2016;22:1049–55.

31. Nerius M, Doblhammer G, Tamgüney G. GI infections are associated with an increased risk of Parkinson’s disease. Gut. 2019;gutjnl-2019-318822.

827 32. Peter I, Dubinsky M, Bressman S, Park A, Lu C, Chen N, et al. Anti-Tumor Necrosis Factor
828 Therapy and Incidence of Parkinson Disease Among Patients With Inflammatory Bowel Disease.
829 JAMA Neurol. 2018;75:939–46.

830 33. Rolli-Derkinderen M, Leclair-Visonneau L, Bourreille A, Coron E, Neunlist M, Derkinderen P. Is
831 Parkinson's disease a chronic low-grade inflammatory bowel disease? J Neurol. 2019;1–7.

832 34. Wan Q-Y, Zhao R, Wu X-T. Older patients with IBD might have higher risk of Parkinson's
833 disease. Gut. 2018;gutjnl-2018-317103.

834 35. Kishimoto Y, Zhu W, Hosoda W, Sen JM, Mattson MP. Chronic Mild Gut Inflammation
835 Accelerates Brain Neuropathology and Motor Dysfunction in α-Synuclein Mutant Mice.
836 Neuromolecular Med. 2019;

837 36. Houser MC, Tansey MG. The gut-brain axis: is intestinal inflammation a silent driver of
838 Parkinson's disease pathogenesis? npj Parkinson's Disease. 2017;3:3.

839 37. Joers V, Masilamoni G, Kempf D, Weiss AR, Rotterman TM, Murray B, et al. Microglia,
840 inflammation and gut microbiota responses in a progressive monkey model of Parkinson's disease: A
841 case series. Neurobiology of Disease. 2020;144:105027.

842 38. Kahle PJ, Neumann M, Ozmen L, Muller V, Jacobsen H, Schindzielorz A, et al. Subcellular
843 localization of wild-type and Parkinson's disease-associated mutant alpha -synuclein in human and
844 transgenic mouse brain. J Neurosci. 2000;20:6365–73.

845 39. Jung S, Aliberti J, Graemmel P, Sunshine MJ, Kreutzberg GW, Sher A, et al. Analysis of
846 fractalkine receptor CX(3)CR1 function by targeted deletion and green fluorescent protein reporter
847 gene insertion. Mol Cell Biol. 2000;20:4106–14.

848 40. Kitazawa M, Oddo S, Yamasaki TR, Green KN, LaFerla FM. Lipopolysaccharide-induced
849 inflammation exacerbates tau pathology by a cyclin-dependent kinase 5-mediated pathway in a
850 transgenic model of Alzheimer's disease. J Neurosci. 2005;25:8843–53.

851 41. Schenk M, Bouchon A, Seibold F, Mueller C. TREM-1--expressing intestinal macrophages
852 crucially amplify chronic inflammation in experimental colitis and inflammatory bowel diseases. J
853 Clin Invest. 2007;117:3097–106.

854 42. Grathwohl SA, Kälin RE, Bolmont T, Prokop S, Winkelmann G, Kaeser SA, et al. Formation and
855 maintenance of Alzheimer's disease β-amyloid plaques in the absence of microglia. Nat Neurosci.
856 2009;12:1361–3.

857 43. Rey NL, George S, Steiner JA, Madaj Z, Luk KC, Trojanowski JQ, et al. Spread of aggregates
858 after olfactory bulb injection of α-synuclein fibrils is associated with early neuronal loss and is
859 reduced long term. Acta Neuropathol. 2017;1–19.

860 44. Schneider CA, Rasband WS, Eliceiri KW. NIH Image to ImageJ: 25 years of image analysis. Nat
861 Methods. 2012;9:671–5.

862 45. Smyth GK. limma: Linear Models for Microarray Data. In: Gentleman R, Carey VJ, Huber W,
863 Irizarry RA, Dudoit S, editors. Bioinformatics and Computational Biology Solutions Using R and
864 Bioconductor [Internet]. New York, NY: Springer New York; 2005 [cited 2019 May 1]. p. 397–420.
865 Available from: https://doi.org/10.1007/0-387-29362-0_23

866 46. Chassaing B, Aitken JD, Malleshappa M, Vijay-Kumar M. Dextran sulfate sodium (DSS)-induced
867 colitis in mice. Curr Protoc Immunol. 2014;104:Unit 15.25.

868 47. Weber B, Saurer L, Schenk M, Dickgreber N, Mueller C. CX3CR1 defines functionally distinct
869 intestinal mononuclear phagocyte subsets which maintain their respective functions during
870 homeostatic and inflammatory conditions. Eur J Immunol. 2011;41:773–9.

871 48. Medina-Contreras O, Geem D, Laur O, Williams IR, Lira SA, Nusrat A, et al. CX3CR1 regulates
872 intestinal macrophage homeostasis, bacterial translocation, and colitogenic Th17 responses in mice.
873 J Clin Invest. 2011;121:4787–95.

874 49. Kostadinova FI, Baba T, Ishida Y, Kondo T, Popivanova BK, Mukaida N. Crucial involvement of
875 the CX3CR1-CX3CL1 axis in dextran sulfate sodium-mediated acute colitis in mice. J Leukoc Biol.
876 2010;88:133–43.

877 50. Kang S, Okuno T, Takegahara N, Takamatsu H, Nojima S, Kimura T, et al. Intestinal epithelial
878 cell-derived semaphorin 7A negatively regulates development of colitis via αvβ1 integrin. J Immunol.
879 2012;188:1108–16.

880 51. Li B, Alli R, Vogel P, Geiger TL. IL-10 modulates DSS-induced colitis through a macrophage-
881 ROS-NO axis. Mucosal Immunol. 2014;7:869–78.

882 52. Prigent A, Lionnet A, Durieu E, Chapelet G, Bourreille A, Neunlist M, et al. Enteric alpha-
883 synuclein expression is increased in Crohn's disease. Acta Neuropathol. 2019;137:359–61.

884 53. Braak H, Del Tredici K, Rüb U, de Vos RAI, Jansen Steur ENH, Braak E. Staging of brain
885 pathology related to sporadic Parkinson's disease. Neurobiol Aging. 2003;24:197–211.

886 54. Neumann M, Kahle PJ, Giasson BI, Ozmen L, Borroni E, Spooren W, et al. Misfolded proteinase
887 K-resistant hyperphosphorylated alpha-synuclein in aged transgenic mice with locomotor
888 deterioration and in human alpha-synucleinopathies. J Clin Invest. 2002;110:1429–39.

889 55. Johnson ME, Stecher B, Labrie V, Brundin L, Brundin P. Triggers, Facilitators, and Aggravators:
890 Redefining Parkinson's Disease Pathogenesis. Trends Neurosci. 2018;S0166-2236:30253–4.

891 56. Braak H, Del Tredici K, Bratzke H, Hamm-Clement J, Sandmann-Keil D, Rüb U. Staging of the
892 intracerebral inclusion body pathology associated with idiopathic Parkinson's disease (preclinical and
893 clinical stages). J Neurol. 2002;249 Suppl 3:III/1-5.

894 57. Shannon KM, Keshavarzian A, Dodiya HB, Jakate S, Kordower JH. Is alpha-synuclein in the
895 colon a biomarker for premotor Parkinson's disease? Evidence from 3 cases. Mov Disord.
896 2012;27:716–9.

897 58. Lebouvier T, Neunlist M, Bruley des Varannes S, Coron E, Drouard A, N'Guyen J-M, et al.
898 Colonic biopsies to assess the neuropathology of Parkinson's disease and its relationship with
899 symptoms. PLoS ONE. 2010;5:e12728.

900 59. Killinger BA, Madaj Z, Sikora JW, Rey N, Haas AJ, Vepa Y, et al. The vermiform appendix
901 impacts the risk of developing Parkinson's disease. Sci Transl Med. 2018;10:eaar5280.

902 60. Kuo Y-M, Li Z, Jiao Y, Gaborit N, Pani AK, Orrison BM, et al. Extensive enteric nervous system
903 abnormalities in mice transgenic for artificial chromosomes containing Parkinson disease-associated
904 α-synuclein gene mutations precede central nervous system changes. Hum Mol Genet. 2010;19:1633–
905 50.

906 61. Luk KC, Kehm V, Carroll J, Zhang B, O'Brien P, Trojanowski JQ, et al. Pathological α-synuclein
907 transmission initiates Parkinson-like neurodegeneration in nontransgenic mice. Science.
908 2012;338:949–53.

62. Van Den Berge N, Ferreira N, Gram H, Mikkelsen TW, Alstrup AKO, Casadei N, et al. Evidence for bidirectional and trans-synaptic parasympathetic and sympathetic propagation of alpha-synuclein in rats. Acta Neuropathol. 2019;

63. Spillantini MG, Schmidt ML, Lee VM, Trojanowski JQ, Jakes R, Goedert M. Alpha-synuclein in Lewy bodies. Nature. 1997;388:839–40.

64. Rey NL, Steiner JA, Maroof N, Luk KC, Madaj Z, Trojanowski JQ, et al. Widespread transneuronal propagation of α-synucleinopathy triggered in olfactory bulb mimics prodromal Parkinson's disease. J Exp Med. 2016;213:1759–78.

65. Puntambekar SS, Davis DS, Hawel L, Crane J, Byus CV, Carson MJ. LPS-induced CCL2 expression and macrophage influx into the murine central nervous system is polyamine-dependent. Brain Behav Immun. 2011;25:629–39.

66. Andus T, Daig R, Vogl D, Aschenbrenner E, Lock G, Hollerbach S, et al. Imbalance of the interleukin 1 system in colonic mucosa—association with intestinal inflammation and interleukin 1 receptor agonist genotype 2. Gut. 1997;41:651–7.

67. Sanchez-Muñoz F, Dominguez-Lopez A, Yamamoto-Furusho JK. Role of cytokines in inflammatory bowel disease. World J Gastroenterol. 2008;14:4280–8.

68. Al-Sadi RM, Ma TY. IL-1beta causes an increase in intestinal epithelial tight junction permeability. J Immunol. 2007;178:4641–9.

69. Capaldo CT, Nusrat A. Cytokine regulation of tight junctions. Biochim Biophys Acta. 2009;1788:864–71.

70. Forsyth CB, Shannon KM, Kordower JH, Voigt RM, Shaikh M, Jaglin JA, et al. Increased Intestinal Permeability Correlates with Sigmoid Mucosa alpha-Synuclein Staining and Endotoxin Exposure Markers in Early Parkinson's Disease. PLOS ONE. 2011;6:e28032.

71. Gray MT, Munoz DG, Gray DA, Schlossmacher MG, Woulfe JM. Alpha-synuclein in the appendiceal mucosa of neurologically intact subjects. Mov Disord. 2014;29:991–8.

72. Labrie V, Brundin P. Alpha-Synuclein to the Rescue: Immune Cell Recruitment by Alpha-Synuclein during Gastrointestinal Infection. JIN. 2017;9:437–40.

73. Kelly LP, Carvey PM, Keshavarzian A, Shannon KM, Shaikh M, Bakay RAE, et al. Progression of Intestinal Permeability Changes and Alpha-Synuclein Expression in a Mouse Model of Parkinson's Disease. Mov Disord. 2014;29:999–1009.

74. Prigent A, Gonzales J, Durand T, Le Berre-Scoul C, Rolli-Derkinderen M, Neunlist M, et al. Acute inflammation down-regulates alpha-synuclein expression in enteric neurons. J Neurochem. 2019;148:746–60.

75. Resnikoff H, Metzger JM, Lopez M, Bondarenko V, Mejia A, Simmons HA, et al. Colonic inflammation affects myenteric alpha-synuclein in nonhuman primates. J Inflamm Res. 2019;12:113–26.

76. Whittem CG, Williams AD, Williams CS. Murine Colitis Modeling using Dextran Sulfate Sodium (DSS). J Vis Exp [Internet]. 2010 [cited 2019 Apr 27]; Available from: https://www.ncbi.nlm.nih.gov/pmc/articles/PMC2841571/

948 77. Erny D, Hrabě de Angelis AL, Jaitin D, Wieghofer P, Staszewski O, David E, et al. Host
949 microbiota constantly control maturation and function of microglia in the CNS. Nat Neurosci.
950 2015;18:965–77.

951 78. Sampson TR, Debelius JW, Thron T, Janssen S, Shastri GG, Ilhan ZE, et al. Gut Microbiota
952 Regulate Motor Deficits and Neuroinflammation in a Model of Parkinson's Disease. Cell.
953 2016;167:1469-1480.e12.

954 79. Chen SG, Stribinskis V, Rane MJ, Demuth DR, Gozal E, Roberts AM, et al. Exposure to the
955 Functional Bacterial Amyloid Protein Curli Enhances Alpha-Synuclein Aggregation in Aged Fischer
956 344 Rats and *Caenorhabditis elegans*. Scientific Reports. 2016;6:34477.

957 80. Wendeln A-C, Degenhardt K, Kaurani L, Gertig M, Ulas T, Jain G, et al. Innate immune memory
958 in the brain shapes neurological disease hallmarks. Nature. 2018;556:332–8.

959 81. Sacino AN, Brooks M, Thomas MA, McKinney AB, Lee S, Regenhardt RW, et al. Intramuscular
960 injection of α-synuclein induces CNS α-synuclein pathology and a rapid-onset motor phenotype in
961 transgenic mice. Proc Natl Acad Sci U S A. 2014;111:10732–7.

962 82. Kim S, Kwon S-H, Kam T-I, Panicker N, Karuppagounder SS, Lee S, et al. Transneuronal
963 Propagation of Pathologic α-Synuclein from the Gut to the Brain Models Parkinson's Disease. Neuron
964 [Internet]. 2019 [cited 2019 Jul 25];0. Available from: https://www.cell.com/neuron/abstract/S0896-
965 6273(19)30488-X

966 83. Lohmann S, Bernis ME, Tachu BJ, Ziemski A, Grigoletto J, Tamgüney G. Oral and intravenous
967 transmission of α-synuclein fibrils to mice. Acta Neuropathol. 2019;

968 84. Uemura N, Yagi H, Uemura MT, Hatanaka Y, Yamakado H, Takahashi R. Inoculation of α-
969 synuclein preformed fibrils into the mouse gastrointestinal tract induces Lewy body-like aggregates in
970 the brainstem via the vagus nerve. Molecular Neurodegeneration. 2018;13:21.

971 85. Svensson E, Horváth-Puhó E, Thomsen RW, Djurhuus JC, Pedersen L, Borghammer P, et al.
972 Vagotomy and subsequent risk of Parkinson's disease. Ann Neurol. 2015;78:522–9.

973 86. Tysnes O-B, Kenborg L, Herlofson K, Steding-Jessen M, Horn A, Olsen JH, et al. Does vagotomy
974 reduce the risk of Parkinson's disease? Ann Neurol. 2015;78:1011–2.

975 87. Braak H, Sastre M, Bohl JRE, de Vos RAI, Del Tredici K. Parkinson's disease: lesions in dorsal
976 horn layer I, involvement of parasympathetic and sympathetic pre- and postganglionic neurons. Acta
977 Neuropathol. 2007;113:421–9.

978 88. Villumsen M, Aznar S, Pakkenberg B, Jess T, Brudek T. Inflammatory bowel disease increases
979 the risk of Parkinson's disease: a Danish nationwide cohort study 1977-2014. Gut. 2018;68:18–24.

980

Figures and figure legends

Grathwohl et al., Figure 1

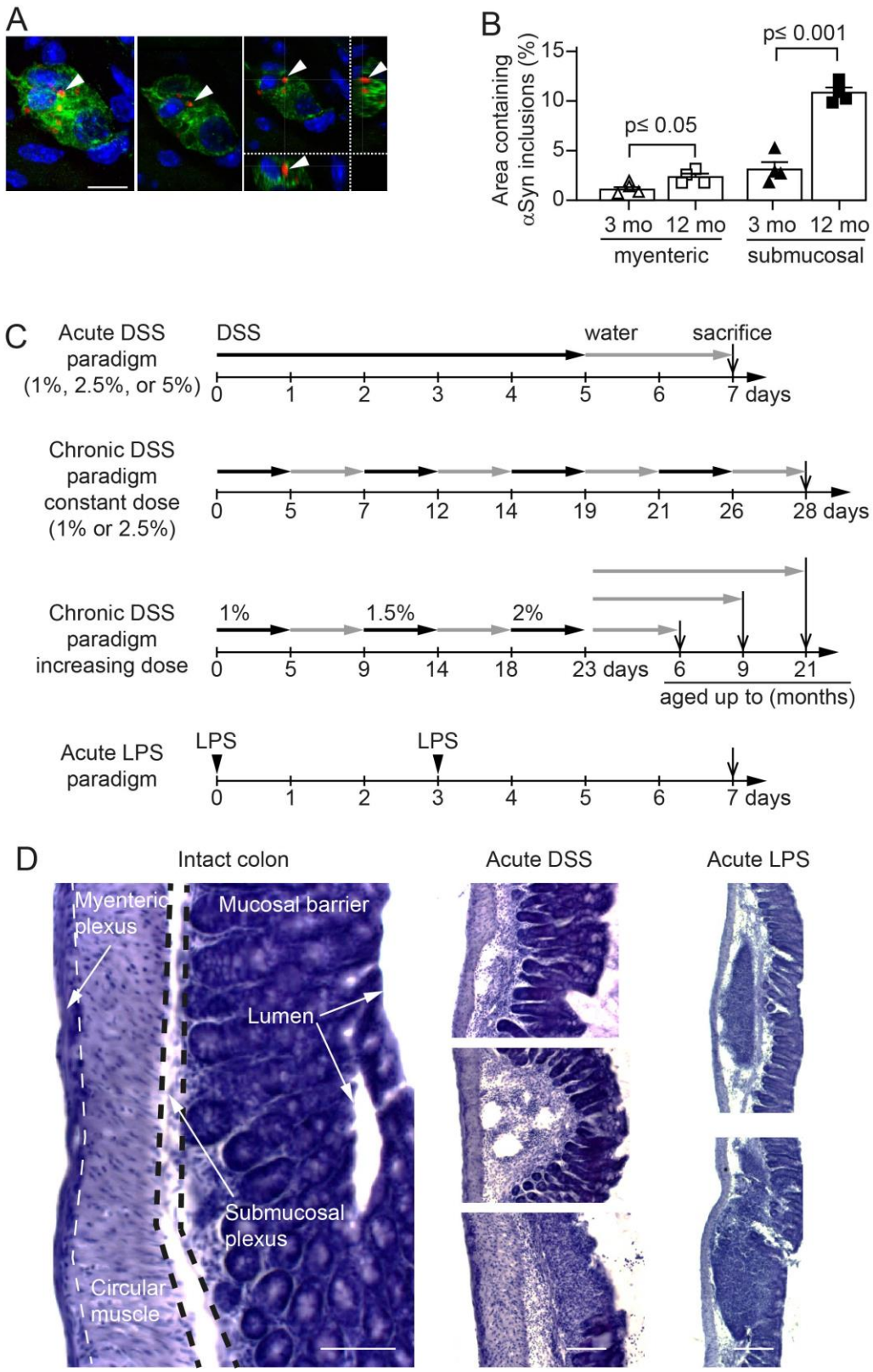

Fig. 1 Age dependent increase of intracellular αSyn accumulation in enteric nervous system of hemizygous (Thy1)-h[A30P]αSyn transgenic mice and setup of the experimental colitis paradigms. a Confocal microscopy imaging of the inclusions of human αSyn (red, antibody clone 211; human αSyn specific) within the ganglia of the submucosal plexus (green, peripherin; blue, DAPI/nuclei) of hemizygous (Thy1)-h[A30P]αSyn transgenic mice. Arrowhead points to one of the typical irregularly sized and shaped αSyn inclusion bodies visualized in 2D z-stacks of rotated confocal images. Scale bar, 100 µm. **b** Stereological quantification of normally occurring human αSyn inclusions in the myenteric and submucosal plexuses of 3 and 12 months old hemizygous (Thy1)-h[A30P]αSyn transgenic mice (n = 4 per group; mean and S.E.M. are shown; Student t-test between the two age groups in each region). **c** Setup of experimental colitis paradigms employing dextran sulfate sodium (DSS, per os in drinking water). Additionally, peripheral inflammation was induced by bacterial lipopolysaccharide (LPS, intraperitoneal injection). After some chronic DSS paradigms mice were aged on normal water up to 6, 9 or 21 months. Mice aged up to 9 or 21 months of age were analyzed for brain pathology **d** Hematoxylin staining of 35 µm thick colon sections of 3 months old hemizygous (Thy1)-h[A30P]αSyn transgenic mice. Organizational layers of the intact colon (left panel). Representative images of various severity degrees of DSS-driven colitis from weak leukocyte infiltration (top panel of acute DSS) to more extensive leukocyte infiltration with mucosal ulceration (lowest panel of acute DSS). Note the different appearance of enteric inflammation in acute LPS-driven peripheral inflammation compared with DSS; e.g., confined immune cell clustering and lymphoid hyperplasia; intact mucosal layer. Scale bar 50 µm (intact colon), 100 µm (acute DSS), and 200 µm (LPS).

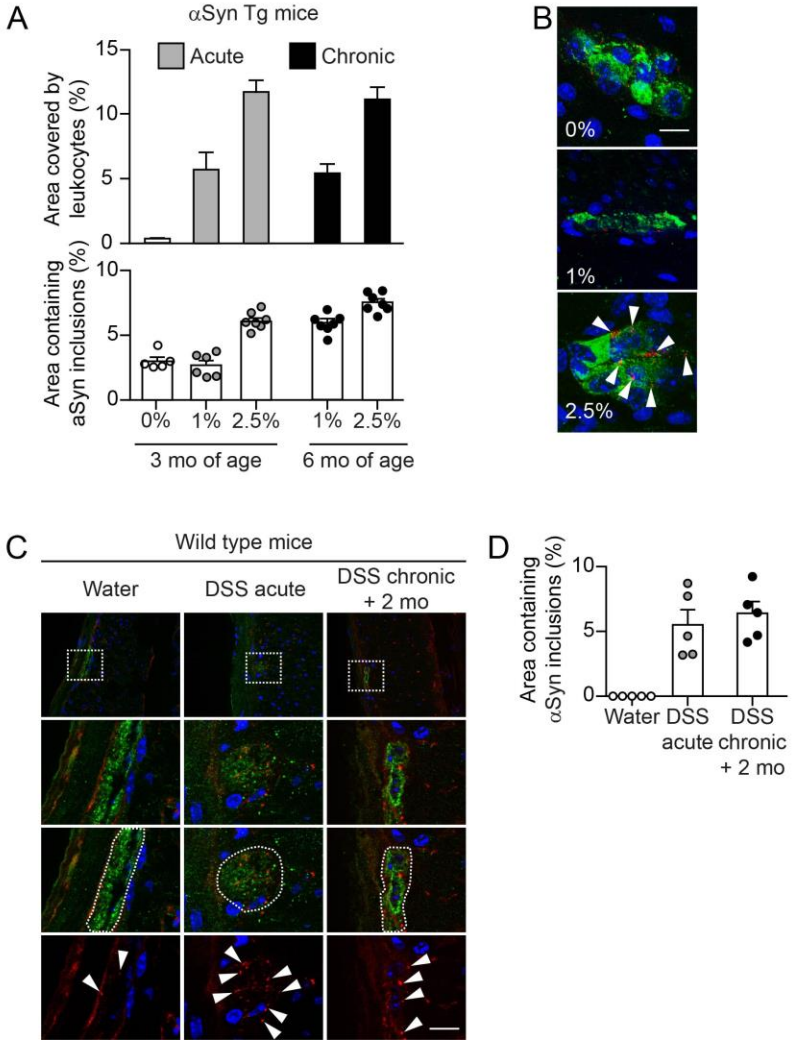

Fig. 2 Colitis severity and duration-dependent aggravation of accumulation of αSyn inclusions in the colonic submucosal plexus of hemizygous (Thy1)-h[A30P]αSyn transgenic and wild type mice. a DSS dose-dependent increase of leukocyte infiltration in the acute and chronic paradigm. The highest acute dose (2.5%) and the two constant chronic doses led to an increase of αSyn inclusions in the submucosal plexus (stereological quantification of αSyn inclusions in the submucosal plexus of 3 and 6 months old hemizygous (Thy1)-h[A30P]αSyn transgenic mice; n = 5-7 per group; mean and s.e.m. are shown). **b** Representative 2D z-stacks of confocal images of increasing abundance of αSyn inclusions (red, human-αSyn specific monoclonal antibody clone 211) in a ganglion of the submucosal plexus (green, peripherin) with cellular nuclei in blue (DAPI) in the acute DSS paradigm. Arrow heads point to the typical irregularly sized and shaped αSyn inclusion bodies that accumulate

in the highest DSS dose. Scale bar 200 µm. **c** Overview of colonic region of 3-month-old wildtype mice (top row) exposed to water or acute DSS (5%) with immunofluorescence analysis of murine αSyn load in the colon performed immediately after colitis or exposed to constant chronic DSS (2.5%) and analysis after aging on normal water for another 2 months. White dotted rectangles in the top row indicate the area that was zoomed out below illustrating in more detail the murine αSyn inclusions (red, rodent αSyn cross-reactive monoclonal antibody syn1/clone 42) in the submucosal plexus (green, peripherin). The lower three rows show DAPI and αSyn inclusions with and without the peripherin channel. The white dotted circled area illustrates the peripherin-positive area that was analyzed for αSyn inclusion bodies (arrow heads in bottom row). Scale bar for the lower three panels 200 µm. **d** Stereological quantification of murine αSyn inclusions in the submucosal plexus of wildtype mice right after acute DSS colitis or after 2 months of recovery from a 4-week chronic DSS colitis (n = 5 per group). Note the regularly arranged and smoothly distributed immunoreactivity for the physiological αSyn with barely any inclusion bodies in the intact enteric nerves of the water group. Statistical analysis for αSyn accumulation was omitted as the noticeable differences between the means are self-evident (error bars indicate standard error of the mean) and an indication for an estimation for significance would be futile.

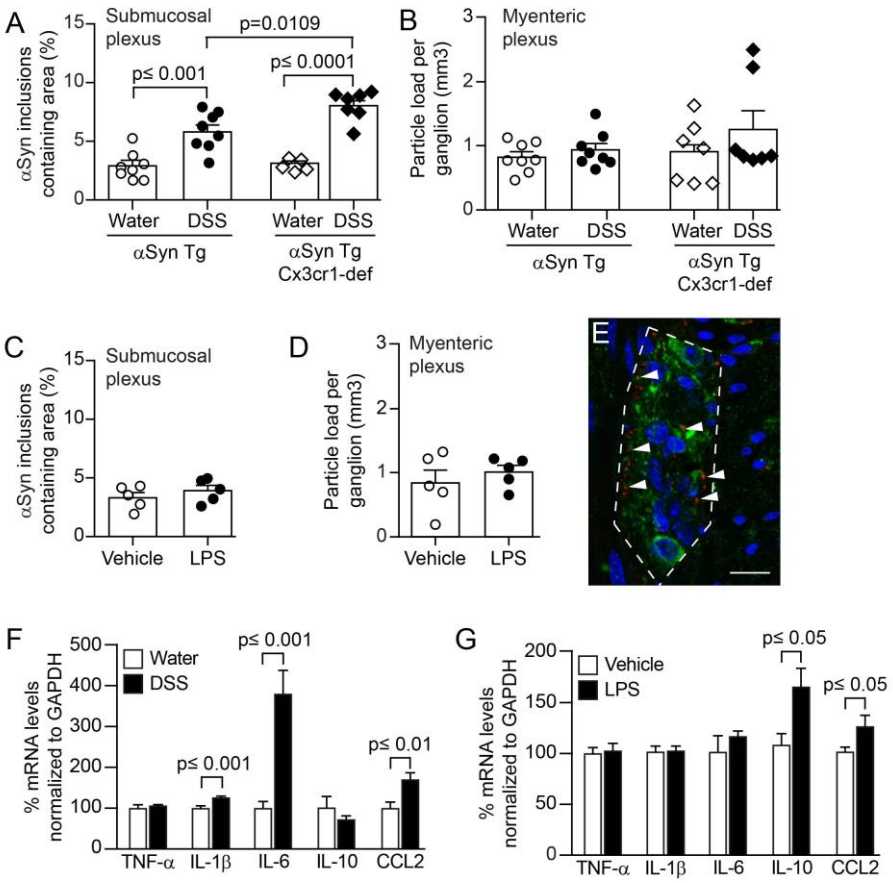

Fig. 3 Colitis induced by peroral DSS but not peritoneal LPS enhances αSyn accumulation in the colonic submucosal plexus of hemizygous (Thy1)-h[A30P]αSyn transgenic mice and can be aggravated by lack of Cx3cr1 signaling. Mice received in an acute paradigm either peroral 5% DSS in their drinking water or intraperitoneally 0.5 mg/kg LPS. Effects of the two agents in the ENS was compared to effects induced by vehicle (see Figure 2C for timelines). Stereological quantification of αSyn inclusions in the submucosal plexus as % area **(a, c)** and in the mucosal plexus as particle load per ganglion **(b, d)** (Two-way ANOVA with Tukey post hoc test; covariates genotype and treatment paradigm). **e** Representative 2D stacks of confocal images of intracellular αSyn inclusions (red, human αSyn specific monoclonal antibody clone 211; arrow heads pointing to some selected inclusions) in a ganglion of the myenteric plexus (green, peripherin) with cellular nuclei in blue (DAPI). Scale bar 50 µm. Gene expression analysis of selected cytokines in the colon of (Thy1)-h[A30P]αSyn transgenic mice that received either acute DSS **(f)** or LPS **(g)** compared to their respective vehicle or water controls. Note the strong increase in IL-6 and the lack of elevation of IL-

10 in the DSS paradigm compared to the LPS paradigm indicating a different inflammatory colonic milieu despite the abundant leukocyte infiltration in both paradigms. N = 5-8 per group; mean and s.e.m.; Student's t-test between inflammatory agent and vehicle for individual cytokines.

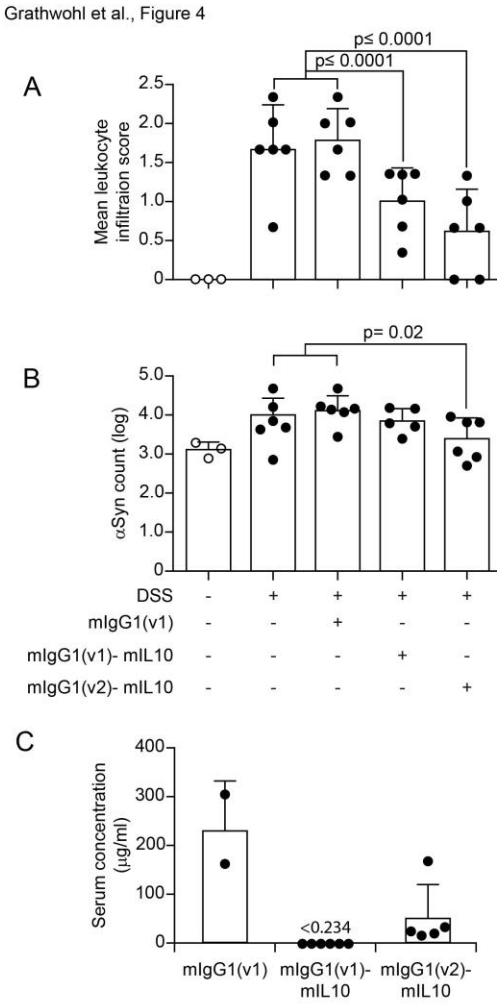

Fig. 4 Systemic IL-10 ameliorates DSS colitis and associated local αSyn accumulation in (Thy1)-h[A30P]αSyn transgenic mice. Two different recombinantly engineered and murine IgG1-fused forms of murine IL-10 (mIgG1(v1)-mIL10 and mIgG1(v2)-mIL10) were administered (150 µg per mouse i.p.) at the beginning of the acute DSS paradigm (5%) in (Thy1)-h[A30P]αSyn transgenic mice. Vehicle and the mIgG1(v1) alone served as untreated controls. **a** Leukocyte infiltration was assessed by visual scoring and (**b)** inclusion features of αSyn were stereologically and semi-automatically quantified and result log scaled for statistical analysis. Both the vehicle group and the

mIgG1(v1) group had similar levels of leukocyte infiltration and αSyn inclusions and were merged for the statistical analysis to compare with the IL-10 treated groups. Both forms of IL-10 ameliorated leukocyte infiltration whereas mIgG1(v2)-mIL10 also blocked the appearance of αSyn inclusions significantly (n = 3-6 per group; mean and s.e.m.; one-way ANOVA and Tukey post hoc test). **a** Persistent exposure mIgG1(v2)-mIL10 versus mIgG1(v1)-mIL10 (lower limit of detection is indicated at <0.234 µg/ml) as measured in serum at the end of the in vivo phase corresponds with beneficial treatment effects on αSyn readout observed above. The mIgG1(v1) was only measured in two mice.

Grathwohl et al., Figure 5

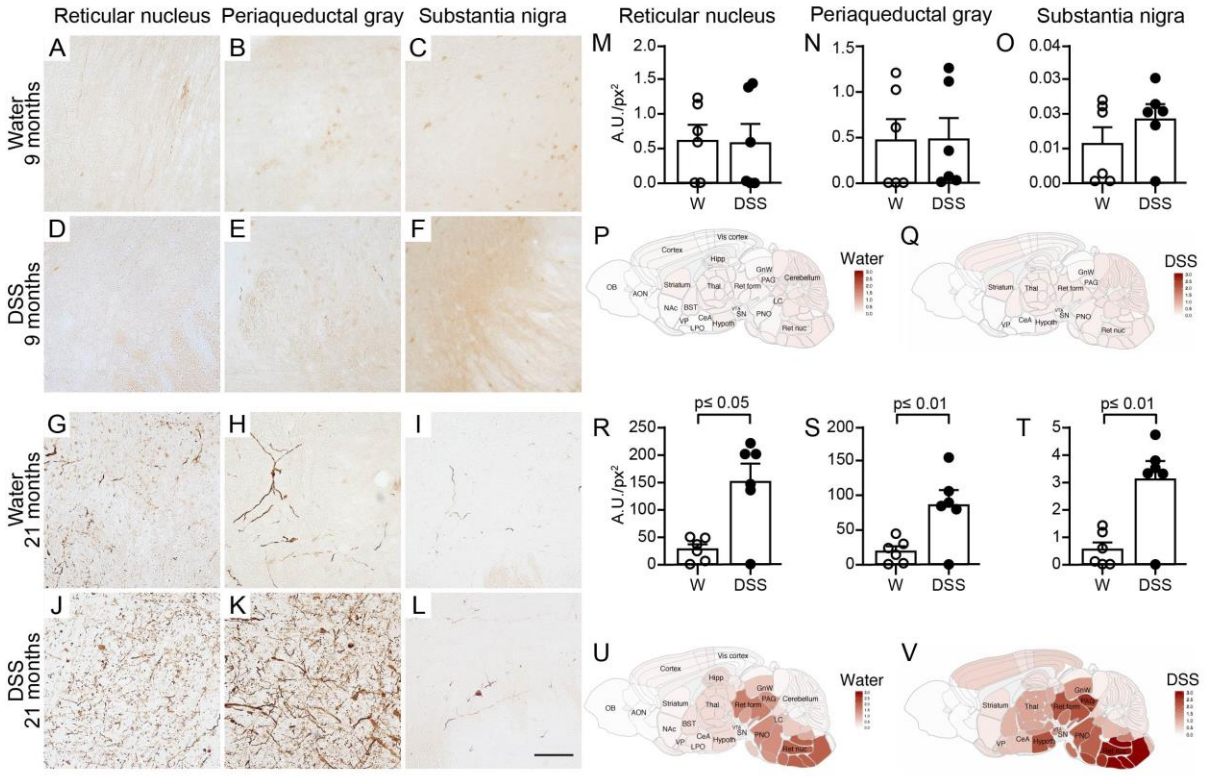

Fig. 5 A single chronic DSS colitis insult causes an age-dependent accumulation of proteinase K resistant pSer129-αSyn in various brain regions of (Thy1)-h[A30P]αSyn transgenic mice. A 3-week chronic increasing dose DSS paradigm was performed with 3-month old (Thy1)-h[A30P]αSyn transgenic mice. After recovering and further aging, various brain regions were analyzed for proteinase K resistant pSer129-αSyn immunoreactivity in 9-month **(a-f)** and 21-month old **(g-l)** mice,

1077 respectively. The dark brown features in G-L indicate proteinase K resistant pSer129-αSyn. They are
1078 barely visible in A-F. Densitometric quantification of pSer129-αSyn immunoreactivity in different
1079 brain regions in 9-month **(m-o)** and 21-month old mice **(r-t)** (n=6 mice per group). The two orders of
1080 magnitude different y-axes between **m**-**o** and **r**-**t** confirm the visual impression in panel **a**-**l**. One 21-
1081 month old DSS-treated mouse was excluded from analysis due to presumed failed treatment; it is
1082 included in the graphs. Statistical analyses were performed using negative-binomial mixed-effects
1083 models adjusting for multiple comparisons. Representative heatmap of the average distribution scores
1084 of pSer129-αSyn immunoreactivity for each treatment group in varying brain regions in all the 9-
1085 month **(p-q)** and 21-month old **(u-v)** mice was generated in a sagittal mouse brain (n=10 mice per
1086 group). Scale bars: 500 μm.
1087
1088

Grathwohl et al., Figure 6

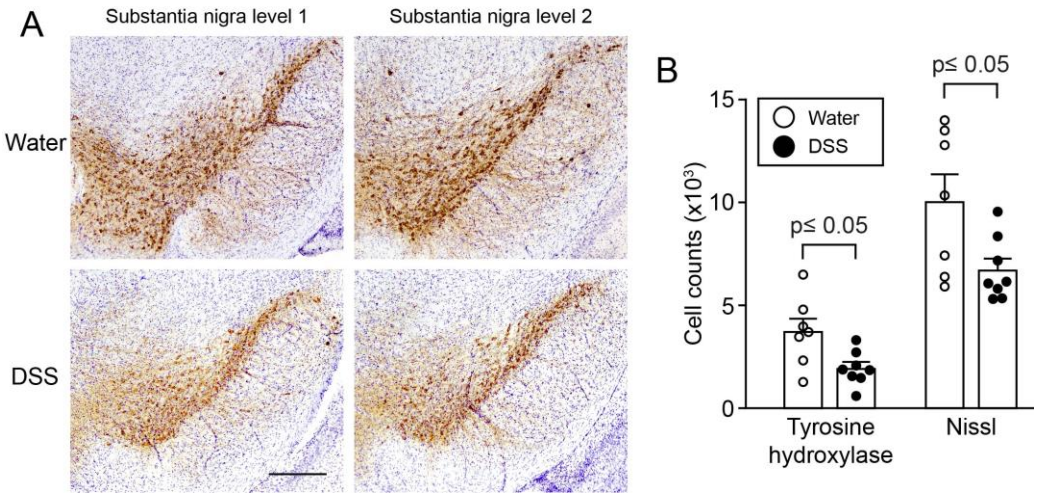

1089
1090 **Fig. 6 Loss of tyrosine hydroxylase and Nissl positive cells in the substantia nigra of (Thy1)-**
1091 **h[A30P]αSyn transgenic mice at 21 months of age, 18 months after DSS colitis.** (Thy1)-
1092 h[A30P]αSyn transgenic mice that were exposed to a chronic DSS-colitis paradigm at 3 months and
1093 were aged to 21 months showed a significant loss of mean count of Nissl-positive cells with tyrosine
1094 hydroxylase (TH) immunoreactivity and cellular Nissl staining in the substantia nigra compared to
1095 age-matched littermate mice in the group that did not experience DSS colitis (water). **a** Representative

images of two levels of the substantia nigra in one mouse per group. **b** Stereological quantification of cells positive for TH or Nissl (n=7-8 mice per group). Statistical analyses of the TH dataset were performed using Student's T-test, while Welch's T-test was used for the Nissl dataset to adjust for unequal variances. Scale bar: 500 μm.

Supplemental Figures

Specific immune modulation of experimental colitis drives enteric alpha-synuclein accumulation and triggers age-related Parkinson-like brain pathology

Stefan Grathwohl[1], Emmanuel Quansah[2], Nazia Maroof[1], Jennifer A. Steiner[2], Liz Spycher[1], Fethallah Benmansour[3], Gonzalo Duran-Pacheco[4], Juliane Siebourg-Polster[4], Krisztina Oroszlan-Szovik[1], Helga Remy[1], Markus Haenggi[1], Marc Stawiski[1], Matthias Sehlhausen[4], Pierre Maliver[4], Andreas Wolfert[5], Thomas Emrich[5], Zachary Madaj[2], Arel Su[4], Martha L. Escobar Galvis[2], Christoph Mueller[6], Annika Herrmann[4], Patrik Brundin[2]*, and Markus Britschgi[1]*

[1] Roche Pharma Research and Early Development, Neuroscience and Rare Diseases Research, Roche Innovation Center Basel, F. Hoffmann-La Roche Ltd, Grenzacherstrasse 124, Basel, Switzerland

[2] Center for Neurodegenerative Science, Van Andel Research Institute, 333 Bostwick Ave. NE, Grand Rapids, MI, USA

[3] Roche Pharma Research and Early Development, pREDi, Roche Innovation Center Basel, F. Hoffmann-La Roche Ltd, Grenzacherstrasse 124, Basel, Switzerland

[4] Roche Pharma Research and Early Development, Pharmaceutical Sciences, Roche Innovation Center Basel, F. Hoffmann-La Roche Ltd, Grenzacherstrasse 124, Basel, Switzerland

[5] Roche Pharma Research and Early Development, Pharmaceutical Sciences, Roche Innovation Center Munich, Roche Diagnostics GmbH, Nonnenwald 2, Penzberg, Germany

[6] Institute of Pathology, University of Bern, Murtenstrasse 31, Bern, Switzerland

Corresponding authors:

* Markus Britschgi, Roche Pharma Research and Early Development, Neuroscience and Rare Diseases Research, Roche Innovation Center Basel, F. Hoffmann-La Roche Ltd, Grenzacherstrasse 124, 4070 Basel, Switzerland

Tel: +41 61 6879116

Email: markus.britschgi@roche.com

* Patrik Brundin, Van Andel Institute, 333 Bostwick Ave. NE, Grand Rapids, MI 49503, USA.

Tel: +1 616.234.5312

Email: patrik.brundin@vai.org

Grathwohl et al., Suppl. Fig. 1

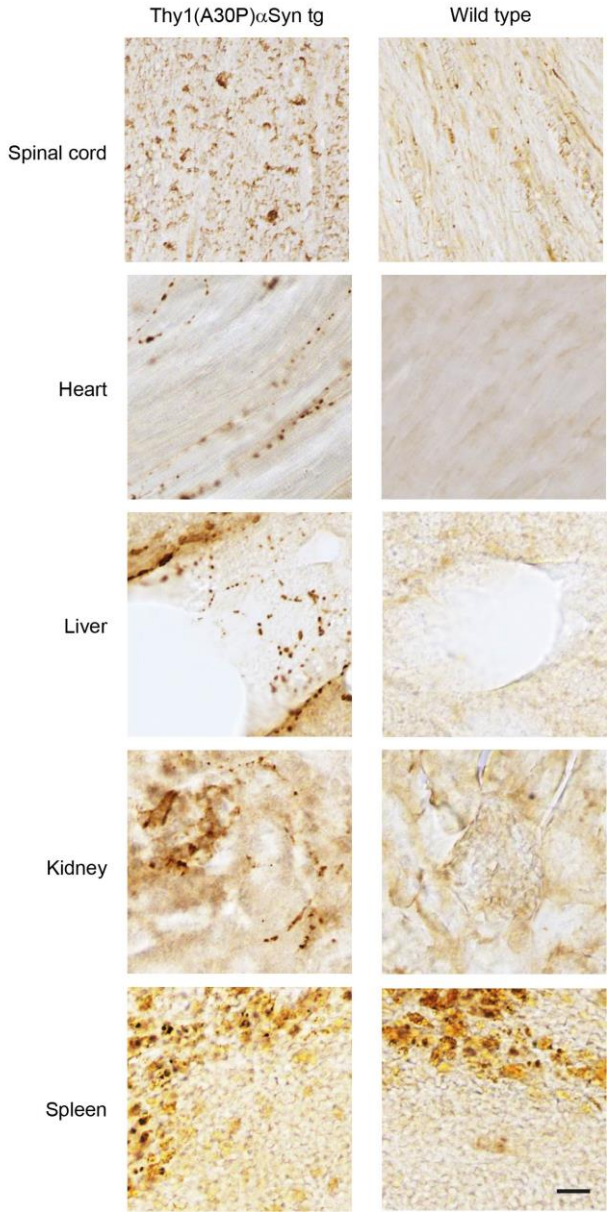

Suppl. Fig. 1 Alpha-synuclein is expressed in majority of organs in wildtype and (Thy1)-h[A30P]αSyn transgenic mice. Immunohistochemical detection of human αSyn (clone LB509 monoclonal antibody) in (Thy1)-h[A30P]αSyn transgenic mice or of endogenous murine αSyn in wildtype mice (syn1 monoclonal antibody) in various organs. Note the typical dot-like structures of the human αSyn in the transgenic mice reminiscent of neuritic inclusions and the very low expression of endogenous murine αSyn in the wildtype mice. The pronounced brownish staining in the spleen is due to the abundant iron which is exposed by the chromogenic staining method. Note, thymocytes in the spleen do not stain for human αSyn supporting the selectivity of the expression of the transgenic

human αSyn under the modified Thy1.2 cassette; e.g. not expressed in thymocytes (See Kahle et al.; reference 26). n = 3 per group Scale bar 20 µm.

Grathwohl et al., Suppl. Fig. 2

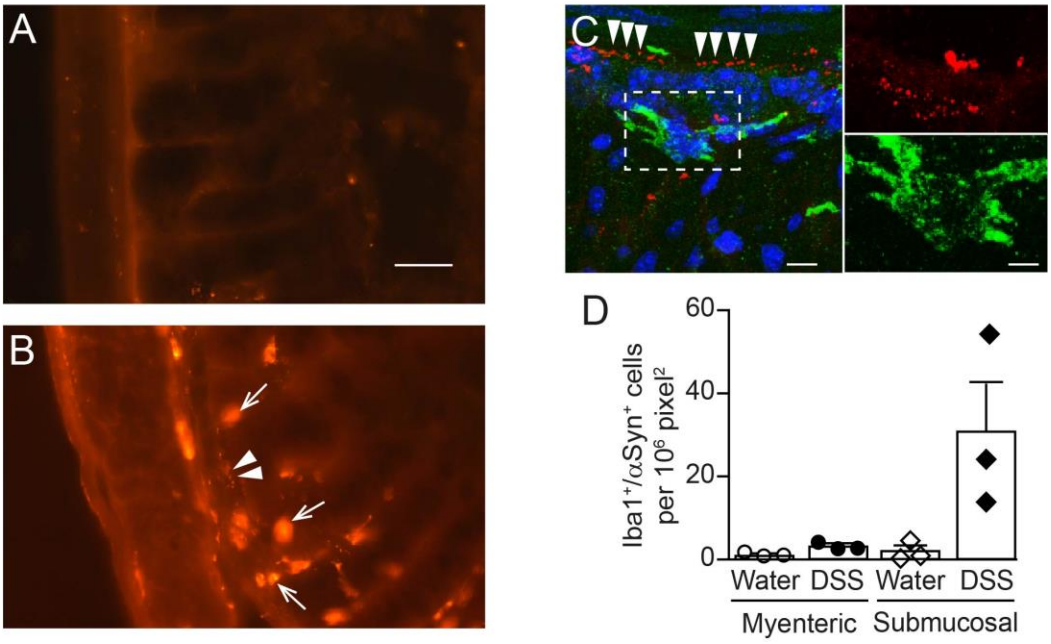

Suppl. Fig. 2 Alpha-synuclein co-localizes with ENS and macrophages upon DSS colitis in αSyn transgenic mice. (A, B) Immunofluorescence image of αSyn staining in colonic region of (Thy1)-h[A30P]αSyn transgenic mice on water **(A)** or after acute DSS colitis (2.5%) **(B)**. Note the small dotted structures of the typical αSyn inclusions in the submucosal plexus (arrow heads) and the large features of immunoreactivity which localize to infiltrating leukocytes (arrows; identified by their typical cellular morphology), similar to what was observed in IBD patients in Figure 1. Scale bar 100 µm. **(C)** 2D stacks and close-up of confocal images co-localizing αSyn (red) with the macrophage marker Iba-1 (green) in the colon of a (Thy1)-h[A30P]αSyn transgenic mouse after DSS colitis. Note the dotted structures of the typical αSyn inclusions in the submucosal plexus (arrow heads). Scale bar 40 µm and 13 µm for the close-up. **(D)** Quantification of numbers of Iba-1/αSyn-double positive macrophages (n = 3 per group; mean and s.e.m.)

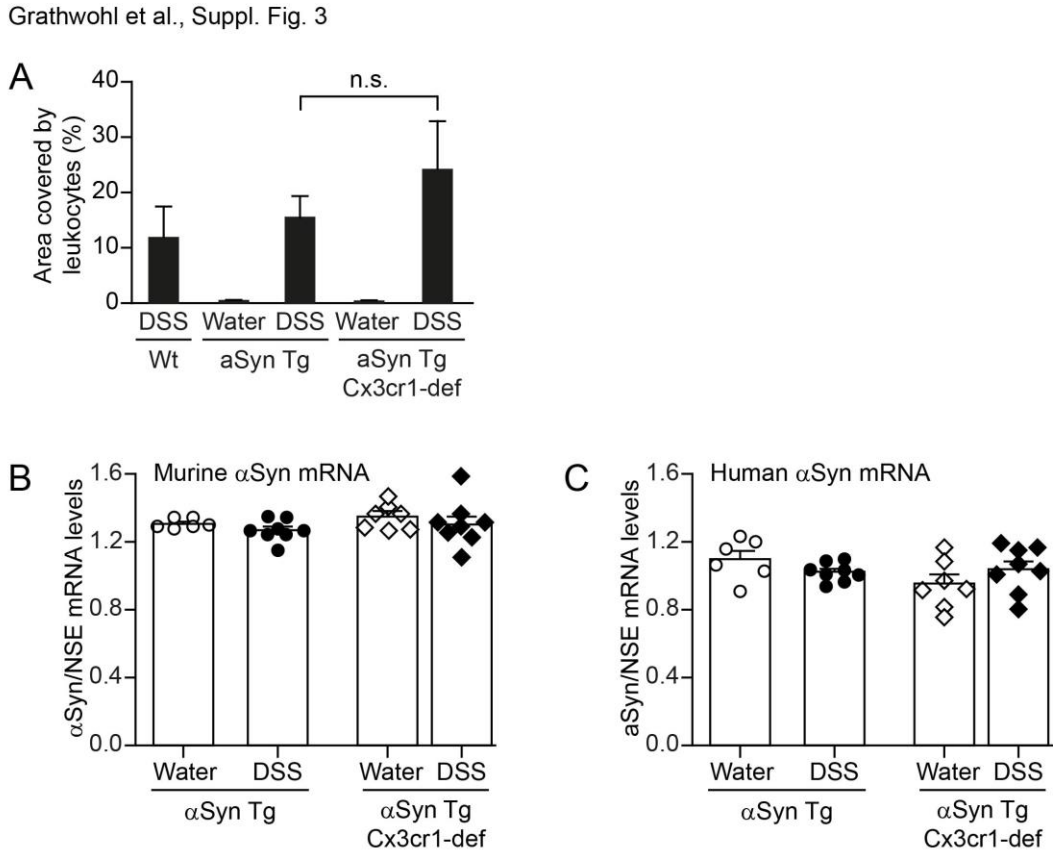

Suppl. Fig. 3 Expression of endogenous and transgenic αSyn in the colon is unchanged after acute DSS colitis. a Administration of DSS (acute 5%) induces leukocyte infiltration in wildtype, (Thy1)-h[A30P]αSyn transgenic (αSyn Tg) and Cx3cr1-deficient (Thy1)-h[A30P]αSyn transgenic mice (αSyn Tg Cx3cr1-def) (Two-way ANOVA with Tukey post hoc test; covariates genotype and treatment paradigm). Expression levels of endogenous murine **(b)** or transgenic human αSyn **(c)** mRNA were normalized to mRNA levels of the neuronal marker neuron specific enolase (NSE) to correct for potential neuronal loss (n = 5-8 per group; mean and s.e.m).

Grathwohl et al., Suppl. Fig. 4

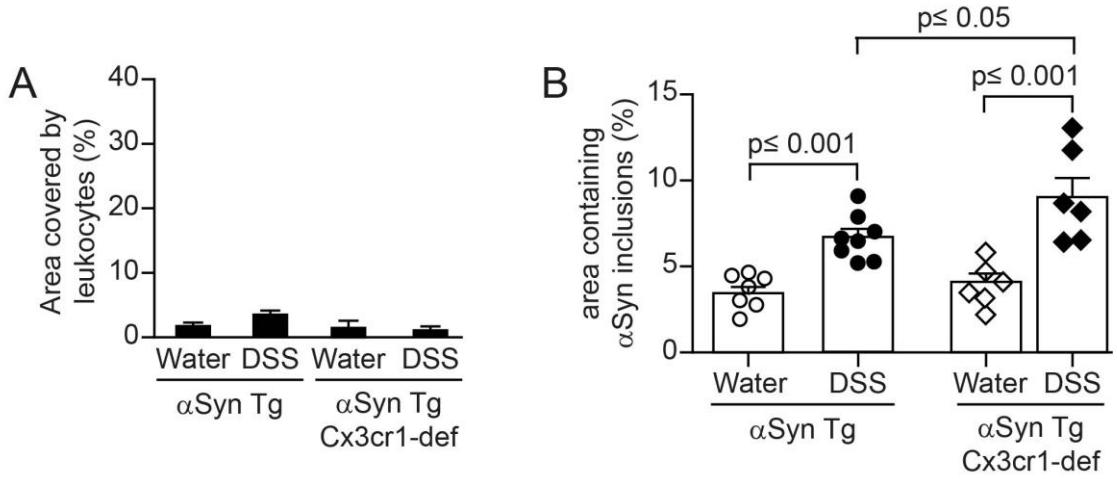

Suppl. Fig. 4 DSS colitis induced accumulation of αSyn in submucosal plexus of (Thy1)-h[A30P]αSyn transgenic mice remain stable long after recovery. A 4-week chronic DSS paradigm was performed with (Thy1)-h[A30P]αSyn (αSyn Tg) and (Thy1)-h[A30P]αSyn crossed with Cx3cr1-def mice (αSyn Tg Cx3cr1-def). After recovery for 2 months and thus analysis at the age of 6 months, **a** the colon was inspected for signs of inflammation (area covered by leukocytes) and **b** amount of αSyn inclusions (area containing αSyn inclusions). N = 6-8 per group. Statistical analyses were performed using two-way ANOVA with Tukey post hoc testing; covariates genotype and treatment paradigm.

Grathwohl et al., Figure S5a

Aged up to 9 months (6 months post a 3-week chronic increasing dose DSS colitis paradigm at the age of 3 months)

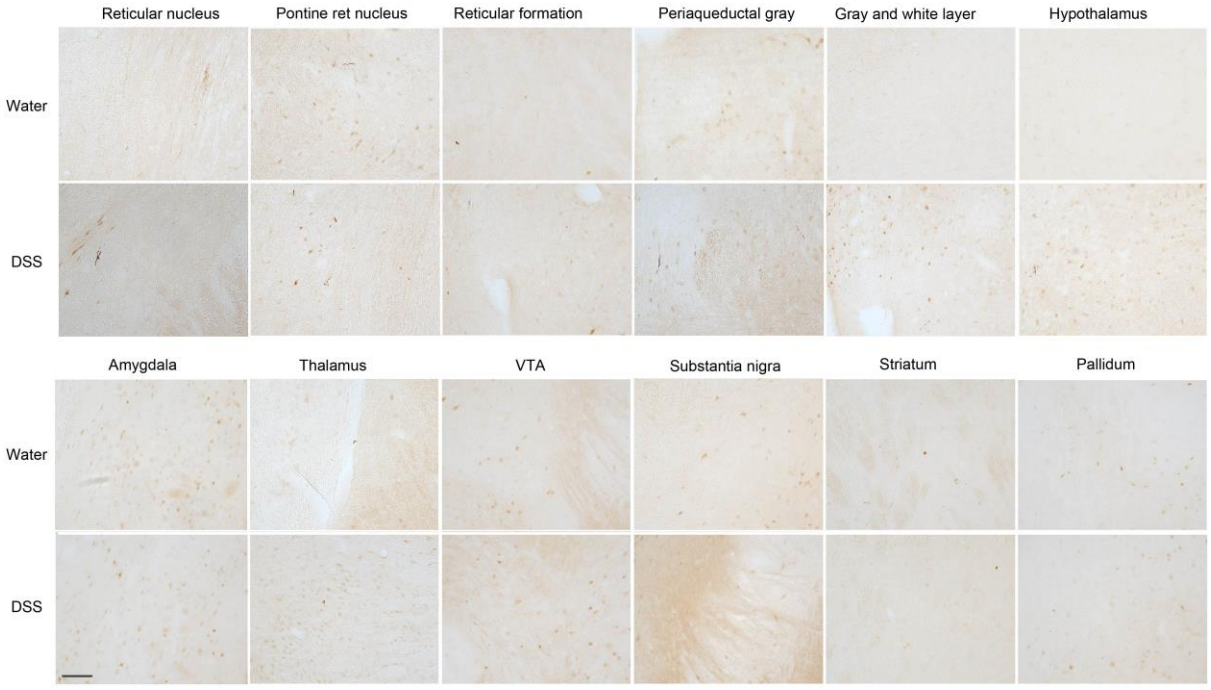

1186

1187

1188

Grathwohl et al., Suppl. Fig. 5b

Aged up to 21 months (18 months post a 3-week chronic increasing dose DSS colitis paradigm at the age of 3 months)

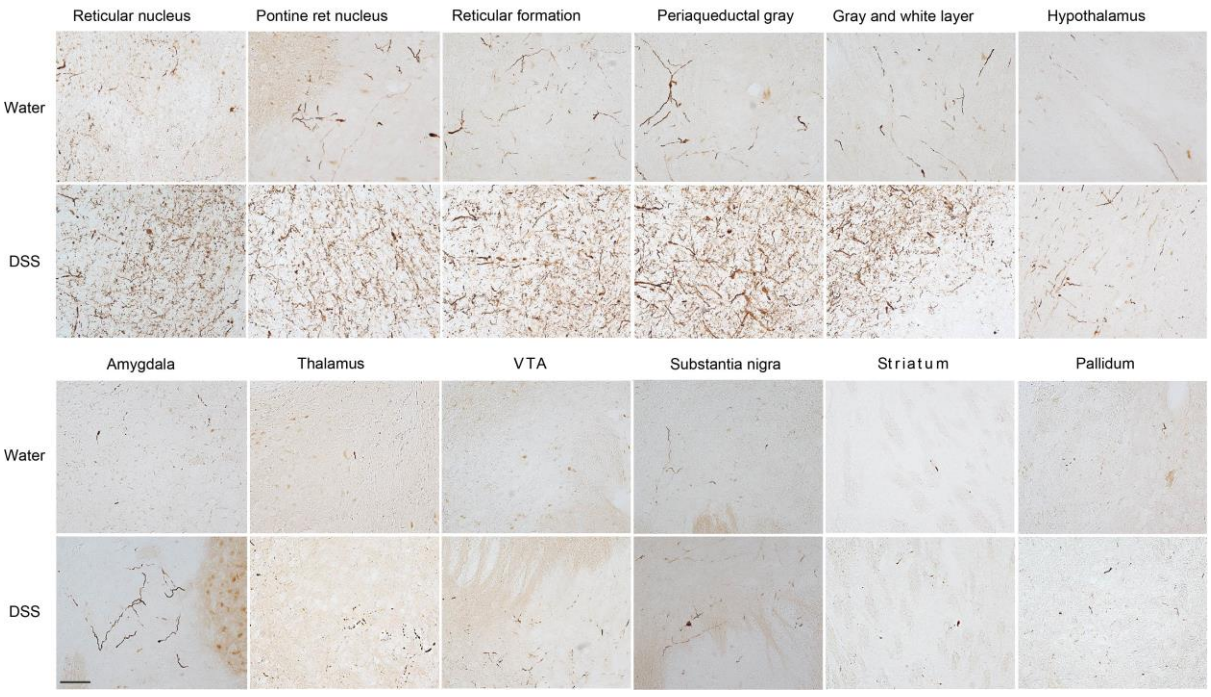

1189

Grathwohl et al., Suppl. Fig. 5c

Quantification of Suppl. Fig. 5b

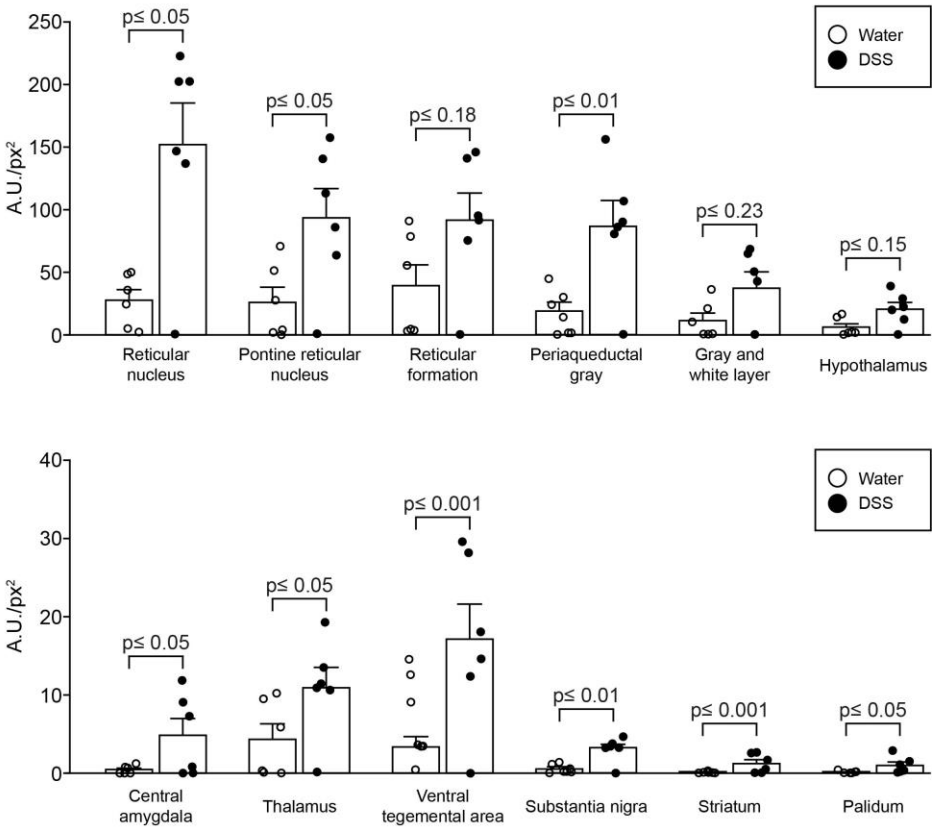

Suppl. Fig. 5 Development of αSyn pathology in the brain of 21-month aged (Thy1)-h[A30P]αSyn transgenic mice upon DSS colitis at young age.

A 3-week increasing dose chronic DSS paradigm was performed with 3-month old (Thy1)-h[A30P]αSyn transgenic mice. After recovery and further aging under normal conditions, various brain regions were analyzed for proteinase K resistant pSer129-αSyn immunoreactivity in 9-month **(a**, cohort 1) and 21-month old **(b**, cohort 2) mice. **c** Densitometric quantification of pSer129-αSyn immunoreactivity in different brain regions in the 21-month old **(from Suppl. Fig 5b)** mice were measured (n=6 mice/group). Statistical analyses were performed using linear mixed-effects model adjusting for multiple comparisons. A.U./px^2, = mean grey value x area stained/total area assessed. Scale bars: 500 µm.

Figures

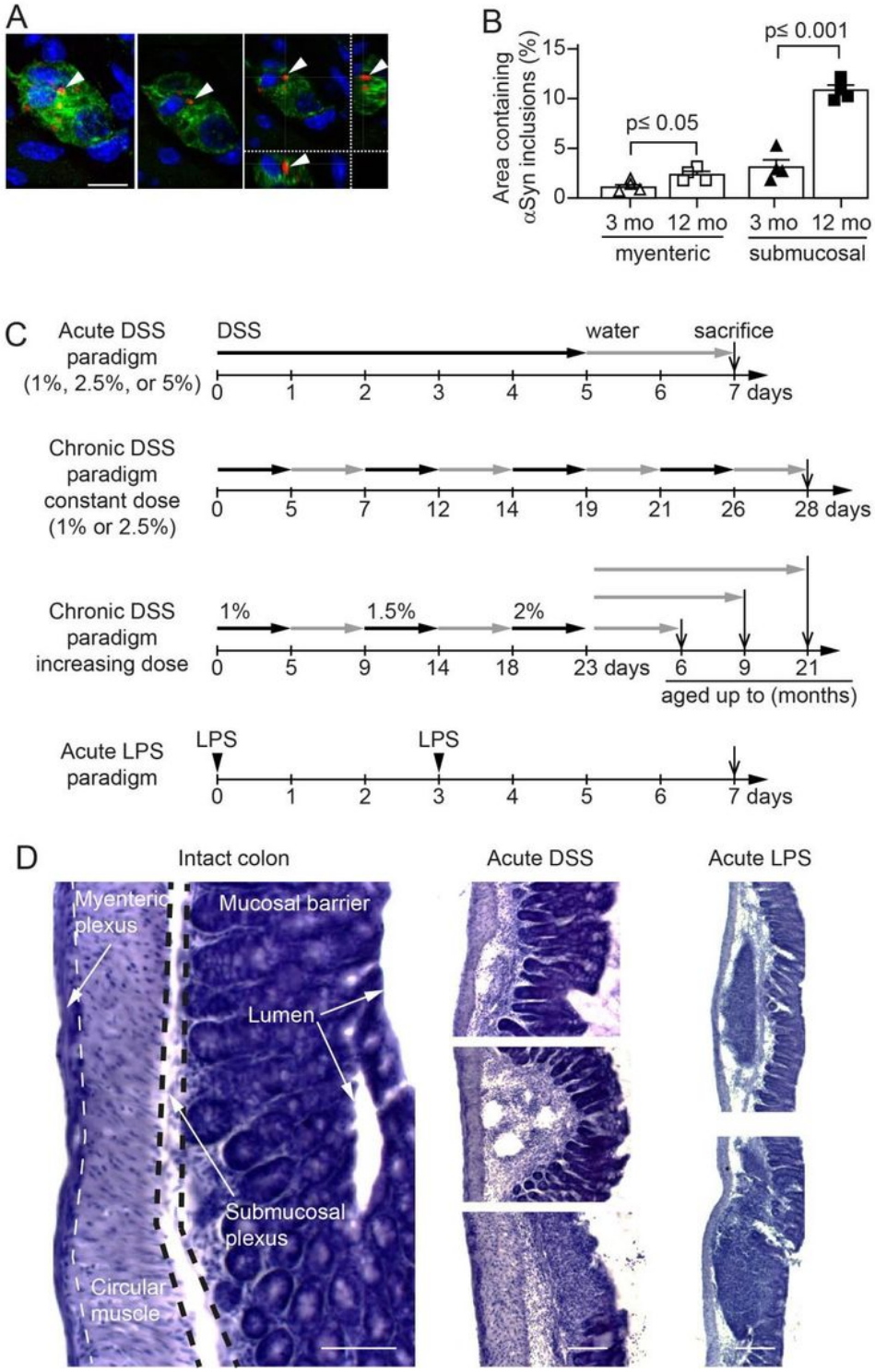

Figure 1

Age dependent increase of intracellular αSyn accumulation in enteric nervous system of hemizygous (Thy1)-h[A30P]αSyn transgenic mice and setup of the experimental colitis paradigms. a Confocal microscopy imaging of the inclusions of human αSyn (red, antibody clone 211; human αSyn specific)

within the ganglia of the submucosal plexus (green, peripherin; blue, DAPI/nuclei) of hemizygous (Thy1)-h[A30P]αSyn transgenic mice. Arrowhead points to one of the typical irregularly sized and shaped αSyn inclusion bodies visualized in 2D z-stacks of rotated confocal images. Scale bar, 100 µm. b Stereological quantification of normally occurring human αSyn inclusions in the myenteric and submucosal plexuses of 3 and 12 months old hemizygous (Thy1)-h[A30P]αSyn transgenic mice (n = 4 per group; mean and S.E.M. are shown; Student t-test between the two age groups in each region). c Setup of experimental colitis paradigms employing dextran sulfate sodium (DSS, per os in drinking water). Additionally, peripheral inflammation was induced by bacterial lipopolysaccharide (LPS, intraperitoneal injection). After some chronic DSS paradigms mice were aged on normal water up to 6, 9 or 21 months. Mice aged up to 9 or 21 months of age were analyzed for brain pathology d Hematoxylin staining of 35 µm thick colon sections of 3 months old hemizygous (Thy1)-h[A30P]αSyn transgenic mice. Organizational layers of the intact colon (left panel). Representative images of various severity degrees of DSS-driven colitis from weak leukocyte infiltration (top panel of acute DSS) to more extensive leukocyte infiltration with mucosal ulceration (lowest panel of acute DSS). Note the different appearance of enteric inflammation in acute LPS-driven peripheral inflammation compared with DSS; e.g., confined immune cell clustering and lymphoid hyperplasia; intact mucosal layer. Scale bar 50 µm (intact colon), 100 µm (acute DSS), and 200 µm (LPS).

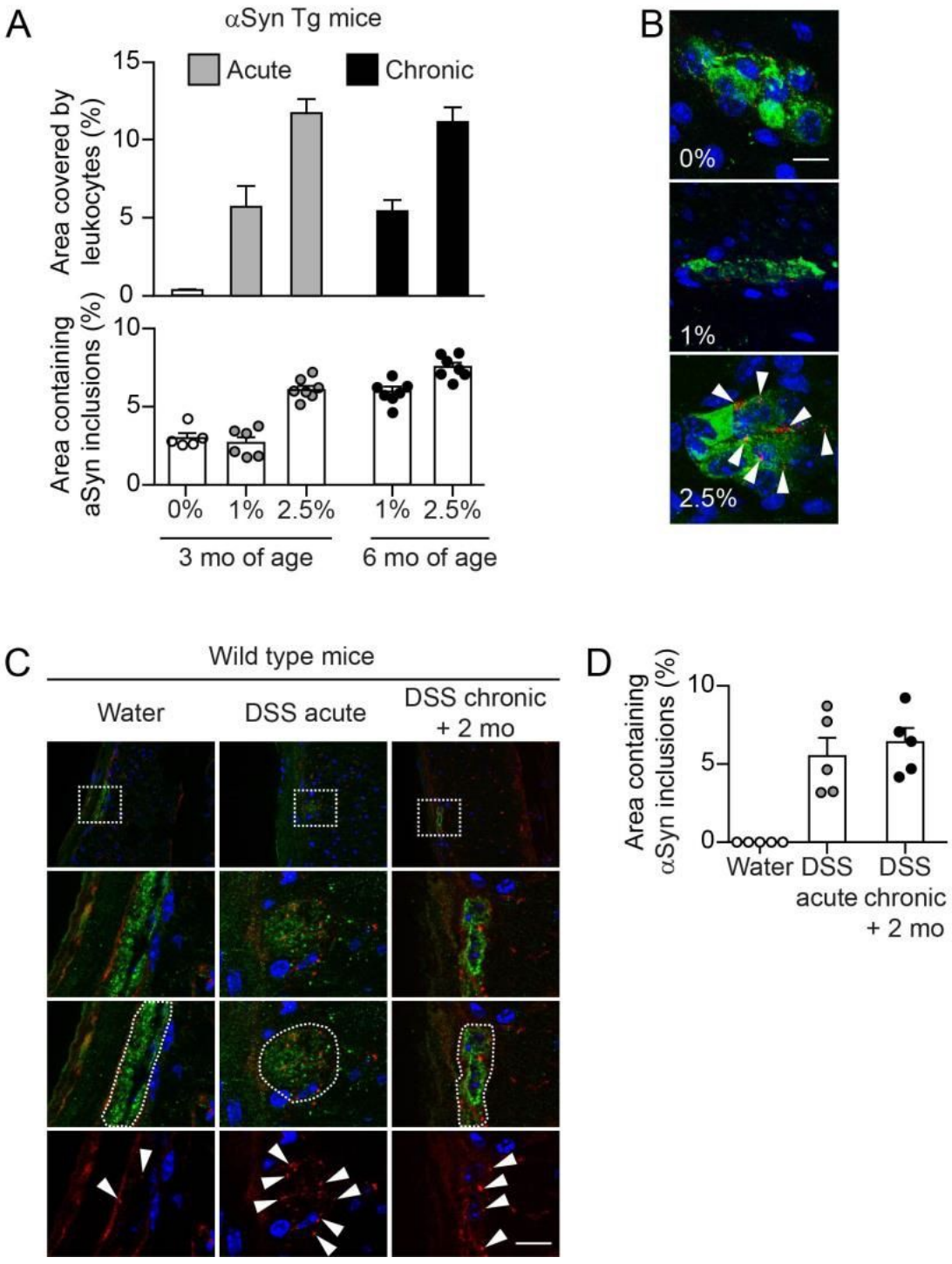

Figure 2

Colitis severity and duration-dependent aggravation of accumulation of αSyn inclusions in the colonic submucosal plexus of hemizygous (Thy1)-h[A30P]αSyn transgenic and wild type mice. a DSS dose-dependent increase of leukocyte infiltration in the acute and chronic paradigm. The highest acute dose (2.5%) and the two constant chronic doses led to an increase of αSyn inclusions in the submucosal plexus (stereological quantification of αSyn inclusions in the submucosal plexus of 3 and 6 months old

hemizygous (Thy1)-h[A30P]αSyn transgenic mice; n = 5-7 per group; mean and s.e.m. are shown). b Representative 2D z-stacks of confocal images of increasing abundance of αSyn inclusions (red, human-αSyn specific monoclonal antibody clone 211) in a ganglion of the submucosal plexus (green, peripherin) with cellular nuclei in blue (DAPI) in the acute DSS paradigm. Arrow heads point to the typical irregularly sized and shaped αSyn inclusion bodies that accumulate Grathwohl et al. in the highest DSS dose. Scale bar 200 μm. c Overview of colonic region of 3-month-old wildtype mice (top row) exposed to water or acute DSS (5%) with immunofluorescence analysis of murine αSyn load in the colon performed immediately after colitis or exposed to constant chronic DSS (2.5%) and analysis after aging on normal water for another 2 months. White dotted rectangles in the top row indicate the area that was zoomed out below illustrating in more detail the murine αSyn inclusions (red, rodent αSyn cross-reactive monoclonal antibody syn1/clone 42) in the submucosal plexus (green, peripherin). The lower three rows show DAPI and αSyn inclusions with and without the peripherin channel. The white dotted circled area illustrates the peripherin-positive area that was analyzed for αSyn inclusion bodies (arrow heads in bottom row). Scale bar for the lower three panels 200 μm. d Stereological quantification of murine αSyn inclusions in the submucosal plexus of wildtype mice right after acute DSS colitis or after 2 months of recovery from a 4-week chronic DSS colitis (n = 5 per group). Note the regularly arranged and smoothly distributed immunoreactivity for the physiological αSyn with barely any inclusion bodies in the intact enteric nerves of the water group. Statistical analysis for αSyn accumulation was omitted as the noticeable differences between the means are self-evident (error bars indicate standard error of the mean) and an indication for an estimation for significance would be futile.

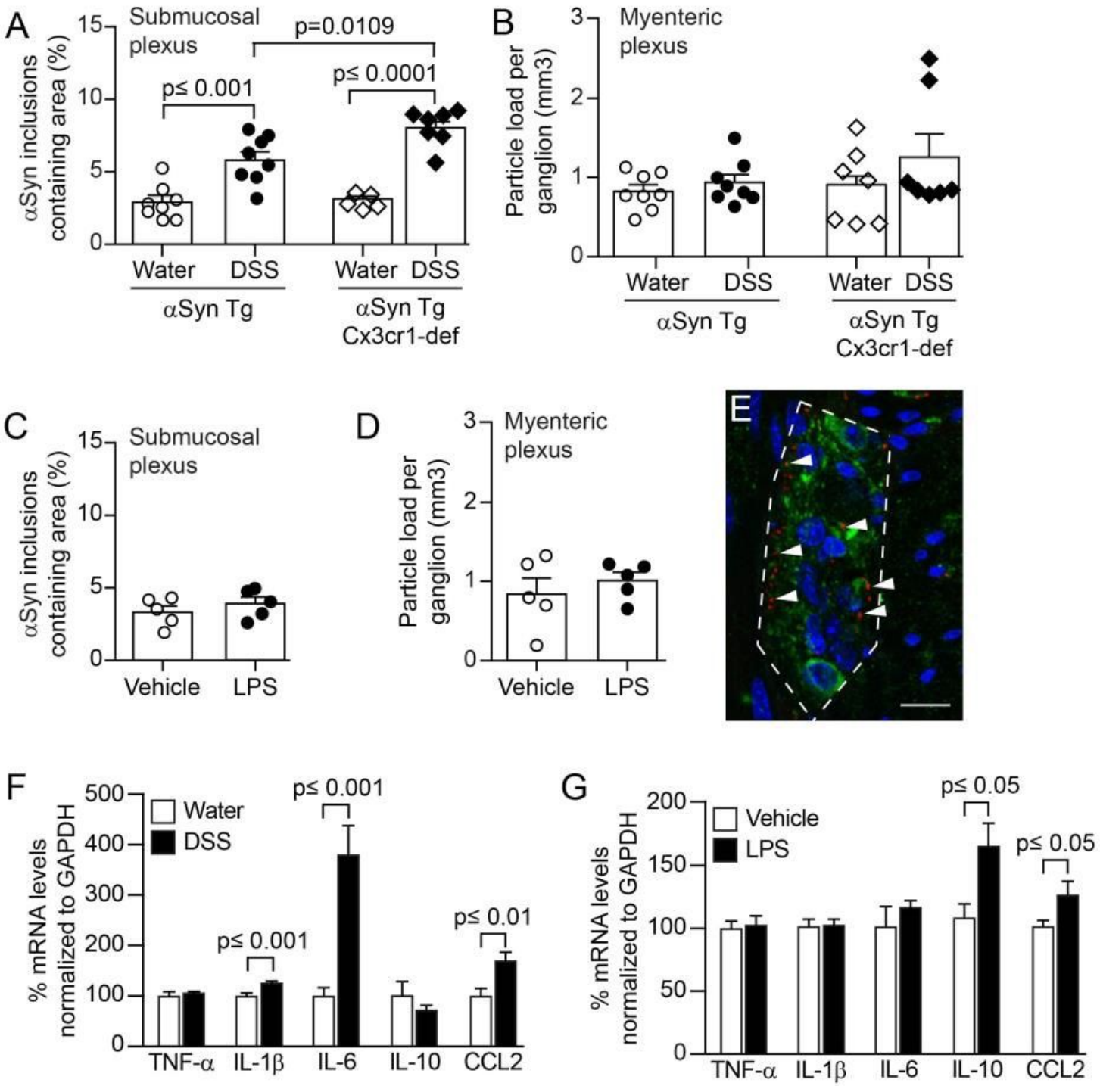

Figure 3

Colitis induced by peroral DSS but not peritoneal LPS enhances αSyn accumulation in the colonic submucosal plexus of hemizygous (Thy1)-h[A30P]αSyn transgenic mice and can be aggravated by lack of Cx3cr1 signaling. Mice received in an acute paradigm either peroral 5% DSS in their drinking water or intraperitoneally 0.5 mg/kg LPS. Effects of the two agents in the ENS was compared to effects induced by vehicle (see Figure 2C for timelines). Stereological quantification of 1αSyn inclusions in the

submucosal plexus as % area (a, c) and in the mucosal plexus as particle load per ganglion (b, d) (Two-way ANOVA with Tukey post hoc test; covariates genotype and treatment paradigm). e Representative 2D stacks of confocal images of intracellular αSyn inclusions (red, human αSyn specific monoclonal antibody clone 211; arrow heads pointing to some selected inclusions) in a ganglion of the myenteric plexus (green, peripherin) with cellular nuclei in blue (DAPI). Scale bar 50 µm. Gene expression analysis of selected cytokines in the colon of (Thy1)- h[A30P]αSyn transgenic mice that received either acute DSS (f) or LPS (g) compared to their respective vehicle or water controls. Note the strong increase in IL-6 and the lack of elevation of IL-Grathwohl et al. 10 in the DSS paradigm compared to the LPS paradigm indicating a different inflammatory colonic milieu despite the abundant leukocyte infiltration in both paradigms. N = 5-8 per group; mean and s.e.m.; Student's t-test between inflammatory agent and vehicle for individual cytokines.

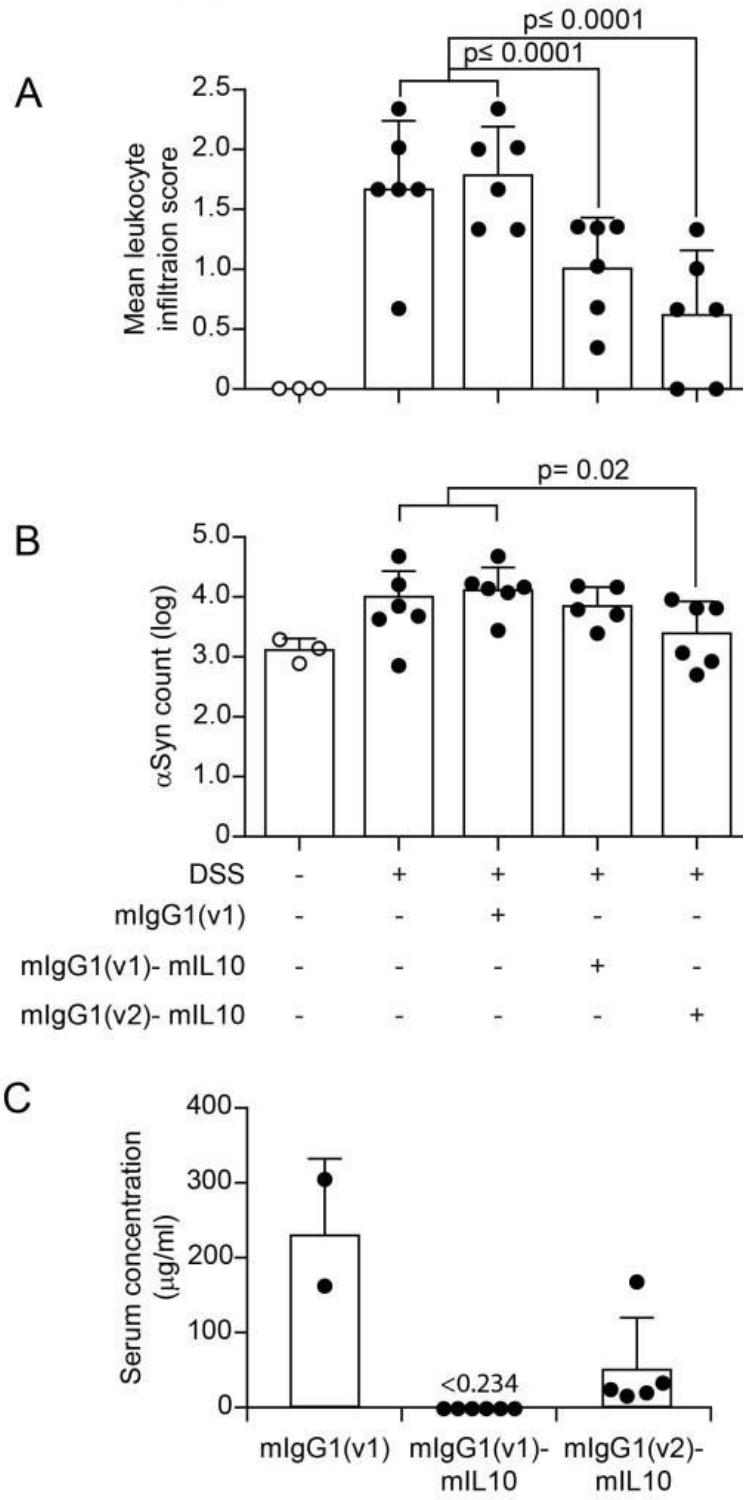

Figure 4

Systemic IL-10 ameliorates DSS colitis and associated local αSyn accumulation in (Thy1)- h[A30P]αSyn transgenic mice. Two different recombinantly engineered and murine IgG1-fused forms of murine IL-10 (mIgG1(v1)-mIL10 and mIgG1(v2)-mIL10) were administered (150 µg per mouse i.p.) at the beginning of the acute DSS paradigm (5%) in (Thy1)-h[A30P]αSyn transgenic mice. Vehicle and the mIgG1(v1) alone served as untreated controls. a Leukocyte infiltration was assessed by visual scoring and (b) inclusion

features of αSyn were stereologically and semi-automatically quantified and result log scaled for statistical analysis. Both the vehicle group and the Grathwohl et al. mIgG1(v1) group had similar levels of leukocyte infiltration and αSyn inclusions and were merged for the statistical analysis to compare with the IL-10 treated groups. Both forms of IL-10 ameliorated leukocyte infiltration whereas mIgG1(v2)-mIL10 also blocked the appearance of αSyn inclusions significantly (n = 3-6 per group; mean and s.e.m.; one-way ANOVA and Tukey post hoc test). a Persistent exposure mIgG1(v2)-mIL10 versus mIgG1(v1)-mIL10 (lower limit of detection is indicated at <0.234 µg/ml) as measured in serum at the end of the in vivo phase corresponds with beneficial treatment effects on αSyn readout observed above. The mIgG1(v1) was only measured in two mice.

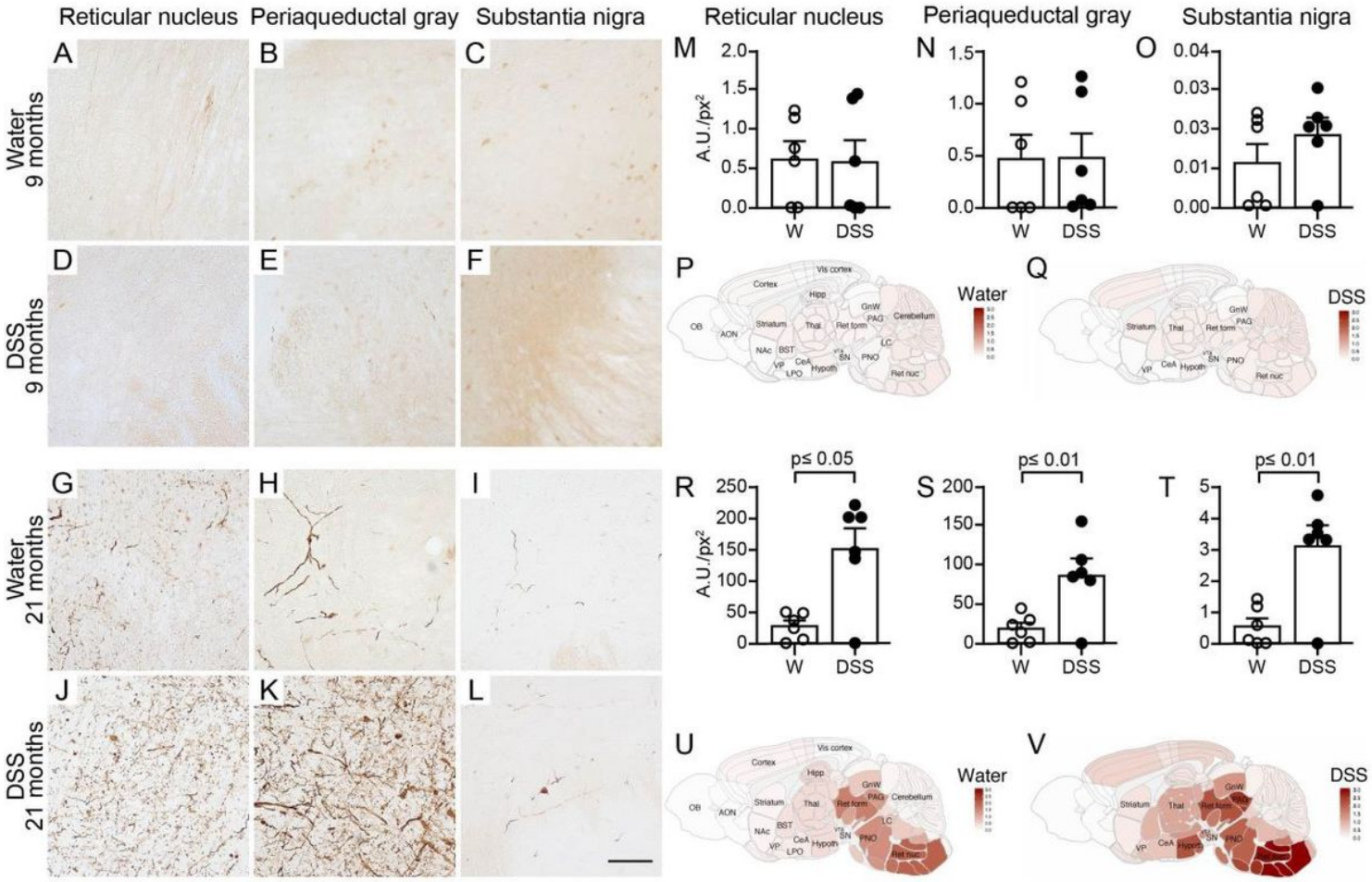

Figure 5

A single chronic DSS colitis insult causes an age-dependent accumulation of proteinase K resistant pSer129-αSyn in various brain regions of (Thy1)-h[A30P]αSyn transgenic mice. A 3-week chronic increasing dose DSS paradigm was performed with 3-month old (Thy1)-h[A30P]αSyn transgenic mice. After recovering and further aging, various brain regions were analyzed for proteinase K resistant pSer129-αSyn immunoreactivity in 9-month (a-f) and 21-month old (g-l) mice, Grathwohl et al. Page respectively. The dark brown features in G-L indicate proteinase K resistant pSer129-αSyn. They are

barely visible in A-F. Densitometric quantification of pSer129-αSyn immunoreactivity in different brain regions in 9-month (m-o) and 21-month old mice (r-t) (n=6 mice per group). The two orders of magnitude different y-axes between m-o and r-t confirm the visual impression in panel a-l. One 21-month old DSS-treated mouse was excluded from analysis due to presumed failed treatment; it is included in the graphs. Statistical analyses were performed using negative-binomial mixed-effects models adjusting for multiple comparisons. Representative heatmap of the average distribution scores of pSer129-αSyn immunoreactivity for each treatment group in varying brain regions in all the 9-month (p-q) and 21-month old (u-v) mice was generated in a sagittal mouse brain (n=10 mice per group). Scale bars: 500 um.

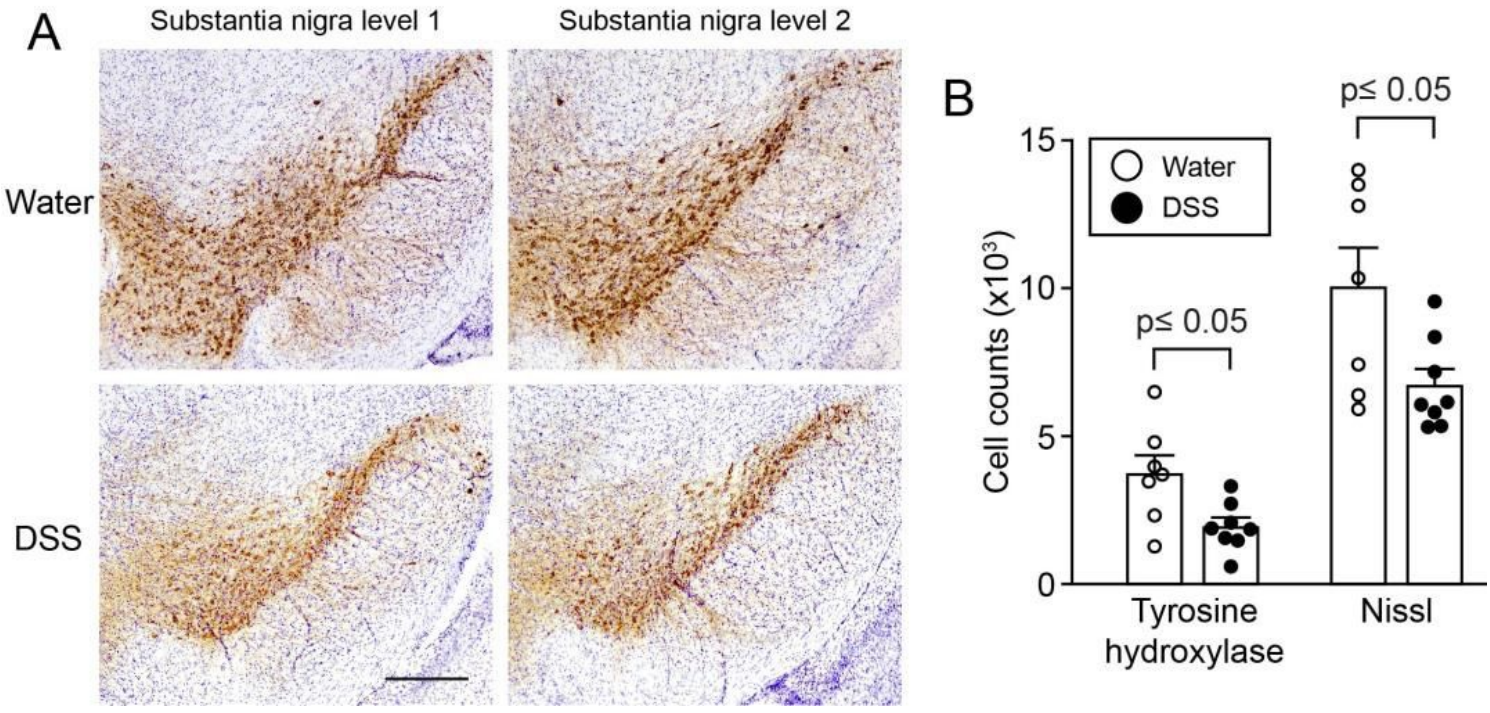

Figure 6

Loss of tyrosine hydroxylase and Nissl positive cells in the substantia nigra of (Thy1)-h[A30P]αSyn transgenic mice at 21 months of age, 18 months after DSS colitis. (Thy1)-h[A30P]αSyn transgenic mice that were exposed to a chronic DSS-colitis paradigm at 3 months and were aged to 21 months showed a significant loss of mean count of Nissl-positive cells with tyrosine hydroxylase (TH) immunoreactivity and cellular Nissl staining in the substantia nigra compared to age-matched littermate mice in the group that did not experience DSS colitis (water). a Representative Grathwohl et al. images of two levels of the substantia nigra in one mouse per group. b Stereological quantification of 1096 cells positive for TH or Nissl (n=7-8 mice per group). Statistical analyses of the TH dataset were 1097 performed using Student's T-test, while Welch's T-test was used for the Nissl dataset to adjust for unequal variances. Scale bar: 500 um.